Structure and Dynamics of Large Ring Polymers

Margarita Kruteva[1], Jürgen Allgaier[1], Michael Monkenbusch[1], Ingo Hoffman[2], Dieter Richter[1]

[1]*Forschungszentrum Jülich GmbH, Jülich Centre for Neutron Science (JCNS-1), 52425 Jülich, Germany*

[2]*Institut Laue-Langevin (ILL), 71 avenue des Martyrs, 38000 Grenoble, France*

Abstract

We report a comprehensive study on the molecular conformation and dynamics of very large polyethylene-oxide (PEO) rings in the melt: (i) For all rings, independent of ring size, by SANS we observe a cross over, from a strong Q-dependence at intermediate Q to a Q^{-2} dependence at higher Q. Constructing a generic model including a cross over from Gaussian statistics at short distances to more compact structures at larger distances, we find the cross over at a distance along the ring of $N_{e,0} = 45 \pm 2.5$ monomers close to the entanglement distance in the linear counterpart. This finding is clear evidence for the predicted elementary loops building the ring conformation. (ii) The radius of gyration $R_g(N)$ follows quantitatively the result of numerous simulations. However, other than claimed, the cross over to mass fractal statistics does occur around $N \cong 10N_{e,0}$, but up to $N \cong 44N_{e,0}$ the relation $R_g(N) \sim N^{0.39}$ holds. The self-similar ring dynamics was accessed by PFG-NMR and NSE: We find three dynamic regimes for center of mass diffusion starting (i) with a strongly sub-diffusive domain $\langle r_{com}^2(t)\rangle \sim t^{\alpha}(0.4 \leq \alpha \leq 0.65)$ (ii) a second sub-diffusive region $\langle r_{com}^2(t)\rangle \sim t^{0.75}$ that (iii) finally crosses over to Fickian diffusion. The internal dynamics at scales below the elementary loop size is well described by ring Rouse motion. At larger scales the dynamics is self-similar and follows very well the predictions of scaling models with preference for the fractal loopy globule (FLG) model. Finally, we note that the key results were previously published in the form of two letters [1,2].

Introduction

In melts of linear chains, the mutual interaction is screened and the chains perform an undisturbed Gaussian random walk. Even though in melts of ring polymers the excluded volume interaction is screened as well, topological constraints that arise from the ring topology remain. Entropically for ring polymers interpenetration is costly and compact structures that evolve for high molecular weight are induced - the ring conformations are assumed to become mass fractals confining rings into territories [3–6].

Polymer melt dynamics is characterized by the fascinating topological interchain interactions that dominate their dynamic behavior. For linear chains topological interactions lead to tube formation that constrains lateral chain motion - in the celebrated reptation process a chain via its ends creeps out of the tube-like constraints imposed by the surrounding chains [7]. Polymer rings don't feature ends. Therefore, they cannot undergo reptation and compared to linear and branched polymers exhibit distinctly different dynamic properties. The ring topology impacts not only the ring conformation but also pertains to the different role of interactions with the surrounding chains. The related phenomena are not only of fundamental interest, but also are highly relevant *e.g.* for a mechanistic understanding of cyclic DNA in chromatin folding in nucleosomes providing thereby easy access to genetic information [8].

Since a long time, the clarification of the detailed nature of the topological constraints and their consequences for the conformation and dynamics of polymer rings has been a challenge both for theoretical and experimental physics including large scale simulation. The inherent problems involved in the synthesis of well-defined rings prevented progress in the field until very recently. Aside of numerous investigations on rings with small N/N_e, where N is the number of monomers and N_e the entanglement distance in the corresponding linear polymer, the largest rings in terms of N/N_e that were investigated so far were polystyrene (PS) rings with $N/N_e \cong 15$ [9] and poly(ethylene oxide) (PEO) rings reaching $N/N_e \cong 10$ [10]. While for PS only structural investigations were performed, for PEO-rings both the conformation as well as the molecular dynamics were studied. For the radius of gyration R_g the PS results indicate $R_g^2 \sim N^{0.94}$ over the entire range of molecular weights, the PEO data display a weaker power law $R_g^2 \sim N^{0.86}$, both being far away from the predicted asymptotic mass fractal behavior $R_g^2 \sim N^{2/3}$.

We studied the conformation and dynamics of very large PEO ring polymers in the melt as a function of their chain length N. In terms of entanglement distances N_e in the corresponding

linear melt we covered sizes from $N \approx 5N_e$ up to $N \approx 44N_e$. This very large range is well beyond what experiments so far achieved and facilitated the direct and clear experimental observation of small-scale, ring size independent substructures with Gaussian conformation. These substructures we take as the signature of elementary loops being at the basis of the self-similar ring conformation [1]. We also investigated the internal motions and the connected short time diffusion properties of these very large polymer rings [2]. Three dynamic regimes for the center of mass (c.o.m.) diffusion were identified. The internal dynamics was found to follow the concept of self-similar motion as proposed in scaling models, in particular Rubinstein's fractal loopy globule (FLG) model [11]. In this manuscript we present data that were partly published previously in the form of two letters [1,2], and put structural and dynamic work into their context. The paper is organized as follows: First we discuss theoretical predictions both for the ring conformation as well for their dynamics. Then we present small angle neutron scattering (SANS) results on the ring conformations followed by the results of dynamic studies that were achieved by neutron spin echo spectroscopy (NSE) and pulsed field gradient (PFG) NMR. Finally, wrapping up the results we conclude about the state of the art.

Theoretical Considerations

a) Ring Conformation

De Gennes first introduced the notion of self-similar fractal crumpled globule conformations of polymers, in order to describe the conformation of collapsed single chains in solution below theta conditions [12]. Under the condition of fixed topological obstacles Rubinstein introduced the double folded lattice animal (DFLA) model for rings [13]. This model considers randomly branched double folded loops that maximize entropy and lead to a fractal dimension $d_f = 4$. In a mean field approach Cates and Deutsch calculated the free energy cost of topological interactions [14]. Thereby they balanced the topological free energy taken as proportional to the overlap parameter O_{CD}: $k_B T O_{CD} \approx k_B T R^3/N v_0$ with the free energy penalty due to confinement: $k_B T N l^2/R^2$. Minimization leads to $R \sim N^{2/5}$ or $d_f = 2.5$ (R: ring size; N: overall chain length; v_0: monomer volume, l: monomer length). Sakaue described the topological constraints in terms of an excluded volume concept called topological volume [15]. It leads to a squeezing of the ring toward a globular state. The onset of compact statistics was estimated to occur around $N^* \approx 10N_e$. The DFLA model was generalized by Grosberg allowing for the interpenetration of loops [16]. The ring conformation then underlies

a skeleton lattice tree branching randomly at the entanglement spacing $d_{tube} \cong l\sqrt{N_e}$, where $l = l_0\sqrt{C_\infty n_b}$ is the monomer length (n_b: number of main chain bonds in a monomer; C_∞ the characteristic ratio; l_0 the bond length). The free energy becomes a function of the backbone length L of the lattice tree with a statistic following a self-avoiding random walk with the fractal dimension $d_b = 5/3$. While for the DFLA $d_f = 4$ and $d_b = 2$, for Grosberg's model $d_f = 3$ and $d_b = 5/3$. Considering rings as a collection of Gaussian loops ranging from N_e to the size of the backbone $\sim N^{2/3}$ that are assembled in random trees, Obukhov *et al.* presented a geometrical model called decorated loop model [17] . For the radius of gyration R_g it predicts:

$$R_g^2 \cong 1.6R_{e,0}^2\left(\frac{N}{N_{e,0}}\right)^{\frac{2}{3}}\left(1 - 0.38\left(\frac{N}{N_{e,0}}\right)^{-\frac{1}{3}}\right) \qquad (1)$$

where $N_{e,0} \approx N_e$ and $R_{e,0}^2 = l^2 N_{e,0}/12$ the radius of gyration of the elementary loop. Eq. (1) describes a very slow cross over to the asymptotic $d_f = 3$ fractal behavior. Finally, conjecturing that the overlap criterion of Kavassalis and Noolandi [18] for entanglement formation in linear melts is also valid for the loop overlap in ring systems Rubinstein et al. developed the FLG model [11]. For linear polymers $O_{KN} \cong \frac{l^3 N_e^{\frac{1}{2}}}{v_0} \approx 20$ was verified for numerous polymer melts in terms of the packing model. Translated to rings the O_{KN}-rule assumes that ring conformations consist of a large loop that stays at the overlap parameter O_{KN} with similar size loops of neighboring rings and a set of smaller loops. The constant overlap O_{KN} of loops is conjectured to occur in a self-similar way over a wide range of length scales from the entanglement length d_{tube} up to ring size $(O_{KN} N v_0)^{1/3}$. Recent simulations by Rosa and Everaers support Rubinstein's conjecture [19] .

Ring conformations also have been subject of numerous simulation approaches. Halverson *et al.* recently rescaled a large number of simulation results in terms of N/N_e resulting in a master curve combining all results for the ring size R_g. They found a common cross over to mass fractal behavior around $N/N_e \cong 15$. From a primitive path analysis of the simulation results by Halverson *et al.* [20,21], Rubinstein *et al.* arrived at a cross over for the characteristic size of the primitive path segment to $d_f = 3$ as a function of the reduced contour length [11].

b) Ring Dynamics

Early work considered the conformation and motion of polymer rings through an array of fixed obstacles. The DFLA model [13] propounded an analogy to randomly branched polymer – the lattice tree, where relaxation occurs by retraction of double folded strands leading to a terminal relaxation time $\tau_d \sim N^3$ with N the number of monomers, fractal dimension of $d_f = 4$ and a center of mass diffusion $D \sim N^{-2}$. Later on, the model was refined correcting the terminal time to $\tau_d \sim N^{2.5}$ [22].

As mentioned above Grosberg *et al.* dismissed the unrealistic limiting fractal dimension of the DFLA model and considered a skeleton lattice tree that branches randomly at an entanglement spacing $d_{tube} = lN_{e,0}^{1/2}$ resulting in the fractal dimension of the backbone or trunk of the lattice tree of $d_p = 5/3$, the statistics of a self-avoiding random walk [16]. For the dynamics of this self-similar structure, Grosberg *et al.* derived $\tau_d \approx \tau_e \left(N/N_{e,0}\right)^{2.56}$, where τ_e is the entanglement time. Finally, the self-consistent FLG model conjecturing that the overlap of loops is limited by an overlap criterion similar to that for linear melts, also leads to a limiting fractal dimension of $d_f = 3$ [11].

In order to discuss the dynamics of such rings in a melt, it is important to note that in a melt of rings the topological constraints are diluting with progressing time, because with time loops of increasing sizes are relaxed and cease to be obstacles in a similar way as tube dilation occurs *e.g.* in polydisperse linear melts [23,24]. The time scale is set by the time a loop of a given size has travelled over its own size defining thereby the effective time dependent tube diameter $d(g,t)$

$$d(g,t) = \langle r_e^2(g) \rangle^{1/2} = \langle \Delta r_{com}^2(g,t) \rangle^{1/2} \qquad (2)$$

where r_e is the diameter of a loop containing g monomers and Δr_{com}^2 is the mean squared displacement of the loop center of mass. The equation holds for complete tube dilation, which is supported by MD-simulations [19]. For $d_f = 3$ $d(g,t)$ becomes $d(g,t) \cong d_0 \left[\frac{g(t)}{N_{e,0}}\right]^{1/3}$ and $d\left(N_{e,0}, \tau_e\right) = d_{tube}$. The FLG model, assuming complete tube dilation, is also termed self-consistent FLG model and leads to

$$\tau_d = \tau_e \left(\frac{N}{N_{e,0}}\right)^{2+1/d_f} \qquad (3)$$

For the c.o.m. diffusion constant the model predicts:

$$D_{com} \cong \frac{R_g^2}{\tau_d} = D_{R,e}\left[\frac{N}{N_{e,0}}\right]^{-2+\frac{1}{d_f}} \tag{4}$$

with $D_{R,e} = {d_{tube}^2}/{\tau_e}$, the Rouse diffusion coefficient of one elementary loop. Without tube dilation in the naive FLG model the terminal times are

$$\tau_d \cong \tau_e\left[\frac{N}{N_{e,0}}\right]^{2+\frac{d_p}{d_f}} \tag{5}$$

and diffusion

$$D_{com} \cong D_e\left[\frac{N}{N_{e,0}}\right]^{-2+\frac{2-d_p}{d_f}} \tag{6}$$

Self-similar relaxation implies that any section of the ring larger than $N_{e,0}$ relaxes in the same way as the whole ring; thus, the FLG model for a mode "p" leads to

$$\tau_p = \tau_e\left[\frac{N}{pN_{e,0}}\right]^{2+1/d_f} \tag{7}$$

and correspondingly for the other models

$$\tau_p \cong \tau_e\left[\frac{N}{pN_{e,0}}\right]^{2+\frac{d_p}{d_f}} \tag{8}$$

Given this property, we call the scaling models also spectral models and the exponents spectral exponents. On the basis of the experimentally determined fractal ring dimensions of the PEO-rings $d_f = 1/\nu$ [1] with small variations owed to slightly different ν, for the spectral exponents the models predict: FLG: 2.45; DFLA: 2.5; Grosberg: 2.75; naive FLG: 2.9.

Aside from theoretical modelling a significant amount of MD-simulations is available. Using coarse grained models, the largest MD-simulation effort so far is due to Halverson *et al.*, where rings up to $57\,N_e$ equivalents were simulated [25]. In some disagreement to the predictions of the scaling models, for ring diffusion they found $D{\sim}N^{-2.3}$. Furthermore, the N-dependencies of ring and linear counterparts were found equal, with the prefactor for ring diffusion about seven times larger than that for linear chains. In agreement with theoretical predictions, for early diffusion the simulation revealed sub-diffusive behavior $\langle r_{com}^2(t)\rangle \sim t^{0.75}$ up to times and distances of about 2 to 3 times R_g. The internal rearrangements of longer rings

were found to occur much faster than the time it takes to diffuse over their own size. But on the other hand, the $t^{1/4}$ regime in the segment self-correlation function extends to 2-3 times of R_g^2; there exists no second $t^{1/2}$ regime as for linear chains [3]. Atomistic simulations on large poly(ethylene oxide) (PEO) rings corresponding to our 10K (M_n= 10 kg/mol) and 20K (M_n= 20 kg/mol) samples were analyzed in terms of Rouse modes that were found to provide an orthogonal basis also for rings [26]. The analysis in terms of Rouse modes revealed that the power law exponent for the Rouse spectrum $\tau_p \sim p^{-2}$ did not change even for the largest ring, while the Rouse amplitudes were diminishing for low p. Very recently Wong and Choi in terms of a united atom model presented MD-simulation for polyethylene (PE) rings in connection with PRISM theory, where aside from normal Fickian diffusion a short time regime with $\langle r_{com}^2(t) \rangle \sim t^{0.42}$ was observed [27].

Ring Synthesis and Characterization

The procedure for the synthesis of the PEO rings up to 20 kg/mol (R10 and R20) is described in reference [28]. In this process the ring formation of HO-PEO-OH is carried out with the help of p-toluenesulfonyl chloride (TosCl) in the presence of KOH. The intermediately formed tosylation product HO-PEO-OTos reacts with still unreacted OH-end groups under the formation of an ether bond. In a dilute solution and considering that the ring closure reaction is much faster than the tosylation reaction, predominantly unimeric rings are formed by reaction of a tosylated chain end with the still OH-functionalized second end of a chain. As the samples were synthesized in gram quantities, the ring closure reactions were carried out at moderate dilution conditions which lead to visible amounts of chain coupling, but the main product was the unimeric ring.

For the synthesis of rings with higher molecular weights than 20 kg/mol (R40 and R100) this procedure was not useful and led to very low ring yields. The main reason for these limitations is the decreasing concentration of reactive groups with increasing molecular weight, which drastically slows down the reactivity in the tosylation step, where OH-PEO-OH reacts with the activation agent TosCl. Therefore, a different strategy was chosen for the synthesis of the R40 and R100 rings. In the new process the linear PEO precursors were synthesized using the potassium salt of di(ethylene glycol) monobenzyl ether (BnO-(EO)2-OK) as initiator for the polymerization of ethylene oxide, yielding mono-alcoholic BnO-PEO-OH. This compound was immediately tosylated with a large excess of TosCl to BnO-PEO-Tos, followed by the cleavage of the initial benzyl group with H2/PdC which leads to HO-PEO-OTos. This

compound was used for the ring closure reactions. The amount of unimeric rings in the cyclization raw products ranged from 30 to 50%, depending on the molecular weight. Unreacted linear precursor and chain coupled higher molecular weight linear byproducts were eliminated from the cyclization raw products by oxidizing the alcoholic chain ends to carboxylic acids and removing the oxidized material with the help of a basic ion exchange resin. Because of the very low concentrations of carboxylic acid head groups in the case of the R40 and R100 polymers, a very fine-grained ion exchange resin (SourceTM 15Q) had to be used in order to efficiently remove the oxidized linear material. Smaller quantities of higher molecular weight cyclic PEO were finally removed by fractionation using chloroform/heptane as solvent/non-solvent pair. Deuterated rings were prepared in the same way as the hydrogenous counterparts and contained as a consequence of the used initiator two hydrogenous EO-units in the ring.

The characterization of the newly synthesized rings hR40, dR40, hR100, and dR100 was performed using size exclusion chromatography (SEC). For all chromatograms there is no higher molecular weight linear or ring shaped polymer visible at lower elution times. The same holds for the linear mother compounds having the same molecular weights as the ring polymers. For all chromatograms, the left flank of the product signal shows no indication of the linear polymer, whose elution time is about 0.5 min. lower than the one of the ring product. In order to test the sensitivity of the SEC method for the detection of linear byproduct, a sample of dR100 was contaminated with 1% of linear polymer. The SEC traces of dR100 and the contaminated sample are shown in Fig. 1. The small shoulder between 18.75 min and 19.25 min shows the linear contamination, which is not present in the non-contaminated sample (see Fig. 1, insert). Therefore, we safely conclude that the fraction of linear chains in the hR40, dR40, hR100, and dR100 ring samples is below 1%. The R10 and R20 samples synthesized earlier contain higher fractions of linear polymer because the purification process of the raw products was less efficient. It should also be pointed out that the quantification of linear chains by NMR end group detection [27] did not work for the R40 and R100 rings because of the extremely small end group concentrations. Table 1 summarizes the obtained ring polymers.

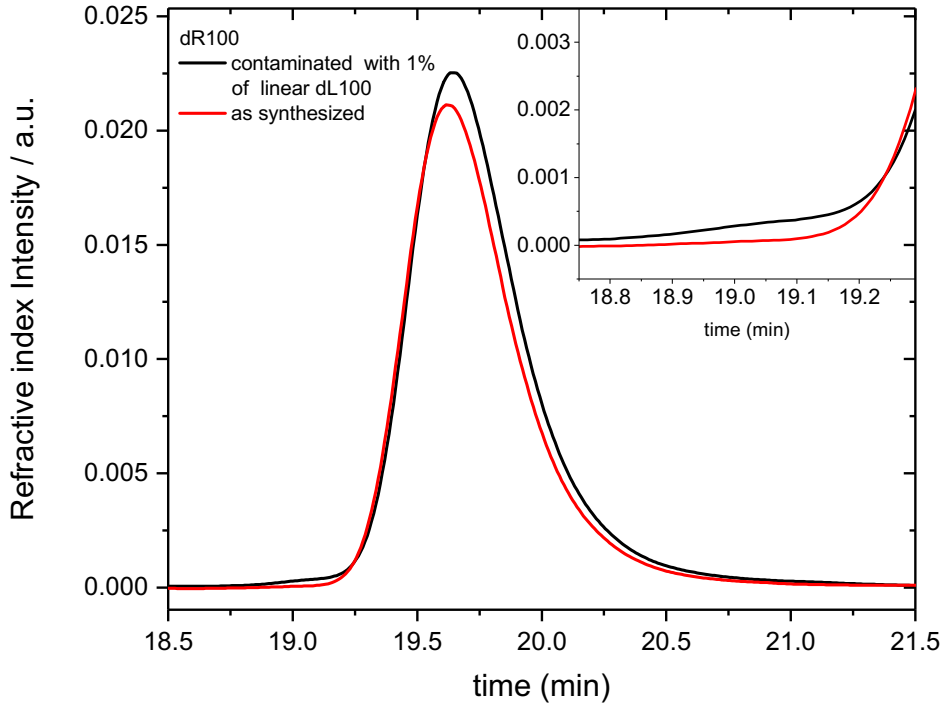

Fig. 1 SEC chromatograms of the ring dR100 with and without 1% of linear dL100. The insert magnifies the region between 18.7 and 19.4 minutes elution time.

Table 1 Molecular weight M_n, number of monomers N, radii of gyration R_g and Bensafi fractal exponent ν of synthesized ring polymers, sub-diffusivity exponent α for the initial c.o.m. diffusion, scaling exponent μ describing the internal ring dynamics, $\langle r_1^2 \rangle$ and $\langle r_2^2 \rangle$ - cross over MSDs of the c.o.m. diffusion. The R_g data were corrected for contribution of linear contaminants, inverse fractal ring dimension $\nu = 1/d_f$.

Ring	M_n [g/mol]	M_w/M_n	N	R_g [nm]	ν	α	μ^{**}	$\langle r_2^2 \rangle$ [nm^2]	$\langle r_1^2 \rangle$ [nm^2]
hR100	83600	1.02	1900						
dL100	94500	1.01	1969						
dR100	94200	1.01	1962	4.90(1)	0.430(3)				
hR100*	87300	1.01	1980	4.92*		0.41(1)	2.4(1)	63.00$^+$	23.00$^+$
dR100*	96000	1.01	2000	4.94*					
hR40	44000	1.01	1000	3.85		0.54(4)	2.4(1)	38.85$^+$	14.24$^+$
dR40	38600	1.01	804	3.54(.1)	0.448(3)				

hR20	20100	1.03	456			0.53(5)	2.5(6)	19.24^{+}	7.40
dR20	21900	1.03	457	2.78(.1)	0.45(1)				
hR10	10100	1.02	230			0.65(4)	5.0(8)	12.00	44.00
dR10	11200	1.02	234	2.14(.04)	0.460(3)				

*the R_g were corrected using $R_g^2 \sim N^{0.78}$, **the scaling model was fitted simultaneously to R40 and R100 ;$^{+}$ scaled cross over MSDs, see text;

Structure Determination

The R40 and R100 samples were based on hydrogenated ring polymer matrices with an addition of small volume fractions ϕ of deuterated rings. In the samples R10 and R20 a small volume fraction of protonated rings was added to the deuterated ring polymer matrix. While the smaller rings R10 (ϕ =5%) and R20 (ϕ =10%) were studied at one volume fraction only, for the large rings a systematic variation of (1%≤ ϕ ≤5%) was performed. The Small Angle Neutron Scattering (SANS) experiments were carried out with the SANS instrument D22 at the ILL in Grenoble at a temperature of 413K [29]. The 2-dimensional SANS data were orientationally averaged, background subtracted and normalized to absolute scale using direct beam measurements. Furthermore, data from adjacent Q values were merged according to their statistical errors.

Figure 2 displays SANS data obtained from all ring samples at the highest volume fraction of deuterated or hydrogenated rings (R10, R20) respectively in a double logarithmic plot. For better visibility the different results were shifted by a factor 2 with respect to each other. All data well display the Guinier range at low Q, a steep decay at intermediate Q and a cross over towards a weaker Q^{-2} dependence at high Q.

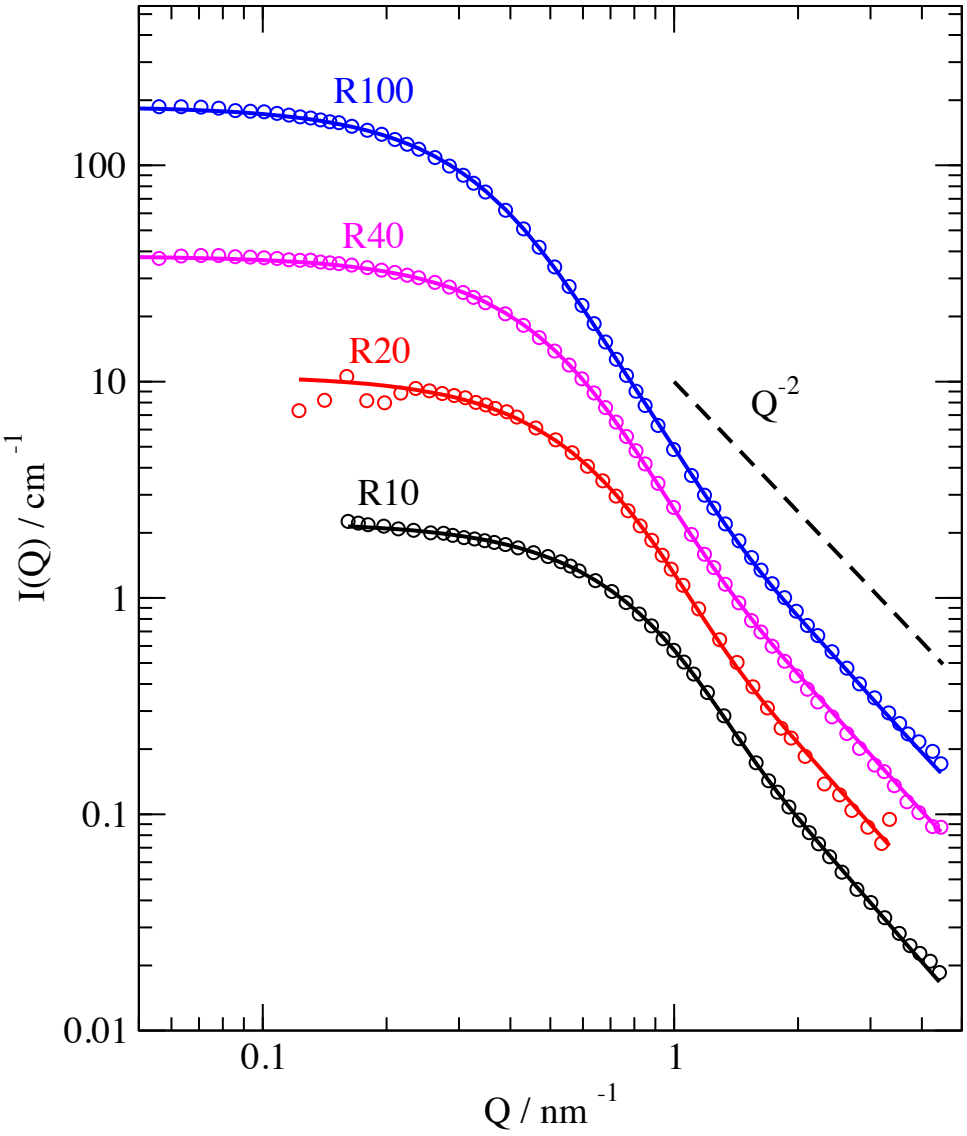

Fig. 2 SANS based form-factors observed for rings of different molecular weights covering the range $5 \leq N/N_{e,0} \leq 44$. For better visibility the data are shifted vertically by a factor of 2 with respect to each other. The solid lines are the results of joint fits with Eqs. 10 (see text). Copyright 2020 ACS

Fig. 3 presents SANS results from the R100 ring taken at different volume fractions of the deuterated component. The data were normalized to the deuterated volume fraction. As may be seen the data perfectly superimpose to each other. Thus, there is no notable Flory-Huggins parameter χ between the hydrogenated and deuterated rings. As χ is negligible for the largest rings, there will be no influence at smaller rings.

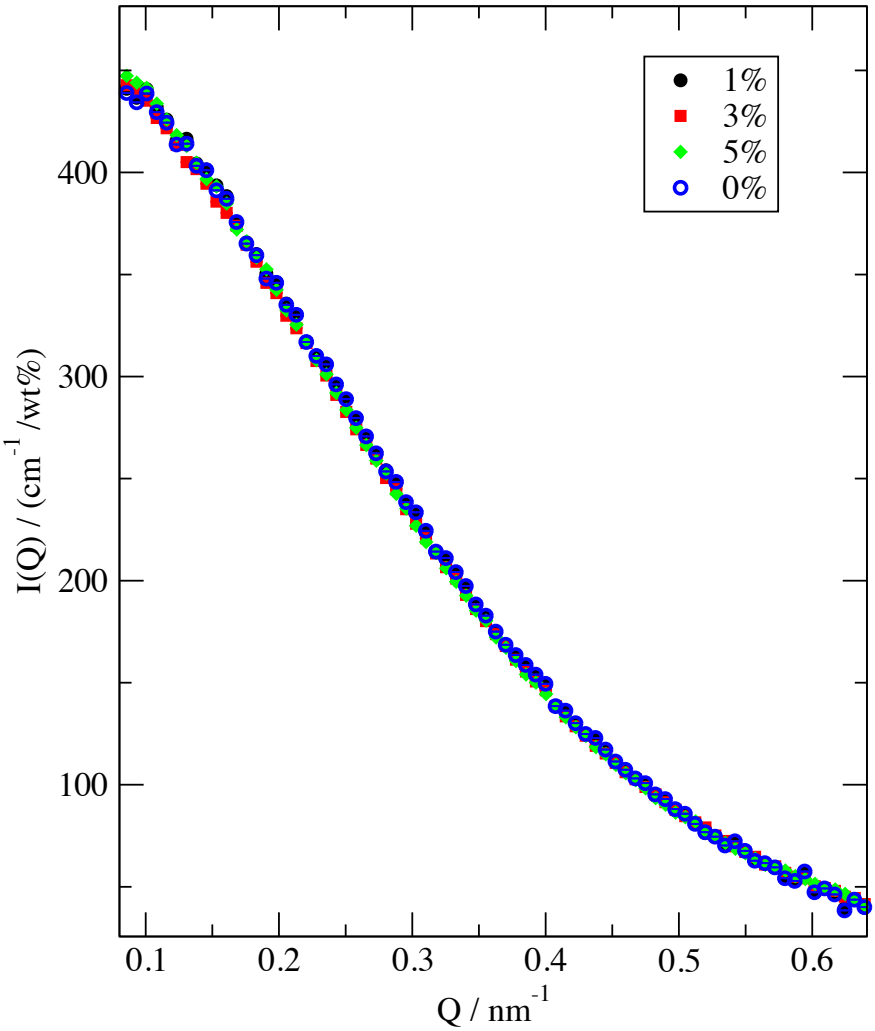

Fig. 3 SANS data for R100 rings normalized to the weight concentration (wt%) and sample volume (see the legend). The data for 0% indicate the SANS intensity extrapolated to zero concentration.

Fig. 4 displays the same data as shown in Fig. 2 in terms of a Kratky plot (multiplication of Y-axis by Q^2) in a range $Q > 0.5$ nm^{-1}. We clearly see a plateau developing at high Q that changes towards a well-defined increase of $I(Q)Q^2$ towards lower Q. The dashed line marks the cross over in Q between the two regimes. We note that the position of this cross over is independent of the ring size and always occurs at the same position in Q. Furthermore, the data show that the clear observation of a well-pronounced crossover effect largely bases on the large ring sizes.

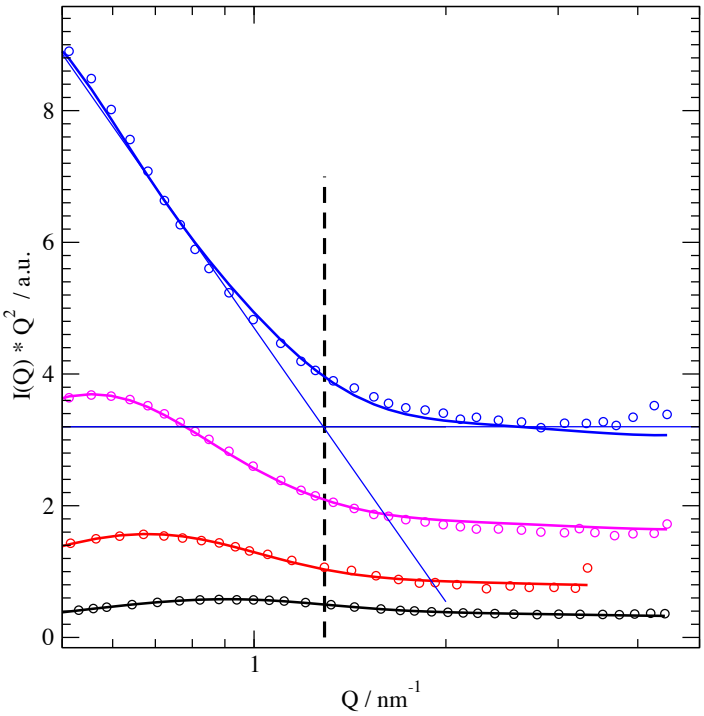

Fig. 4 Kratky plot $I(Q)Q^2$ *vs.* Q of the data displayed in Fig. 2 in the regime of large $Q >$ 0.5 nm^{-1} taking again the same vertical shifts. The dashed line marks the position of the cross over between the fractal and Gaussian regimes. Copyright 2020 ACS

Considering the theoretical ideas of ring conformations built from elementary loops of a molecular size close to that of an entanglement strand in linear melts, we are led to identify the observed cross over as the structural footprint of these elementary loops that need to be independent of the ring size.

Based on these ideas, in the following we construct a generic expression for the ring form-factor that takes in to account this cross over. At large distances along the ring contour length we expect compressed conformations. There the real space distances r between monomers *i* and *j* relate to a monomer random walk more compact than Gaussian with a fractal dimension $d_f = \frac{1}{\nu}$:

$$\langle r^2 \rangle \sim \left((|i-j|) \left(1 - \frac{|i-j|}{N} \right) \right)^{2\nu} \tag{9}$$

with the exponent $\nu < \frac{1}{2}$. For mass fractals with a fractal dimension $d_f = 3, \nu = \frac{1}{d_f} = \frac{1}{3}$. The second term in Eq. 9 arises from the ring closure condition. The common exponentiation of both terms bases on an investigation by Bensafi *et al.* [30] For $|i-j| \leq N_{e,0}$ Gaussian statistics prevails and $\nu = \frac{1}{2}$ holds. We consider a smooth cross over between both regimes and describe it by a sum of Fermi functions of width ν_{width} centered at $N_{e,0}$. Then the ring form factor becomes:

$$P(Q) = \frac{1}{N}\sum_{i,j}^{N} \exp\left[-\frac{Q^2 l^2}{6}|i-j|^{2\nu_{eff}}\left(1-\frac{|i-j|}{N}\right)^{2\nu_{eff}}\right] \tag{10a}$$

with

$$\nu_{eff} = \nu_1 + \left(\frac{\nu - \nu_1}{1+\exp\left(\frac{N_{e,0}-|i-j|}{\nu_{width}}\right)}\right) \tag{10b}$$

where $\nu_1 = \frac{1}{2}$ is the local chain expansion exponent and $\nu = 1/d_f$ the large scale expansion exponent.

The solid lines in Fig. 2 are the result of a joint fit of Eqs. 10 to the corrected SANS data. Thereby the length of the Gaussian substructures $N_{e,0}$ was varied jointly, while the other parameters: total intensity, fractal exponent ν and monomer length l were varied independently. In addition, to correct small mistakes in the background subtraction a flat background was considered that turned out to be in the 10^{-3} regime. With this approach a nearly perfect fit for all rings was achieved. For the crucial size of the Gaussian substructures taken as elementary loop size, we found $N_{e,0}$=45±2.5.

In order to investigate the statistical uncertainty of the elementary loop size, we calculated the residual sum of errors χ^2 for different fixed values of $N_{e,0}$. Fig. 5 displays χ^2 as a function of $N_{e,0}$ showing a well-defined minimum at $N_{e,0} = 45$.

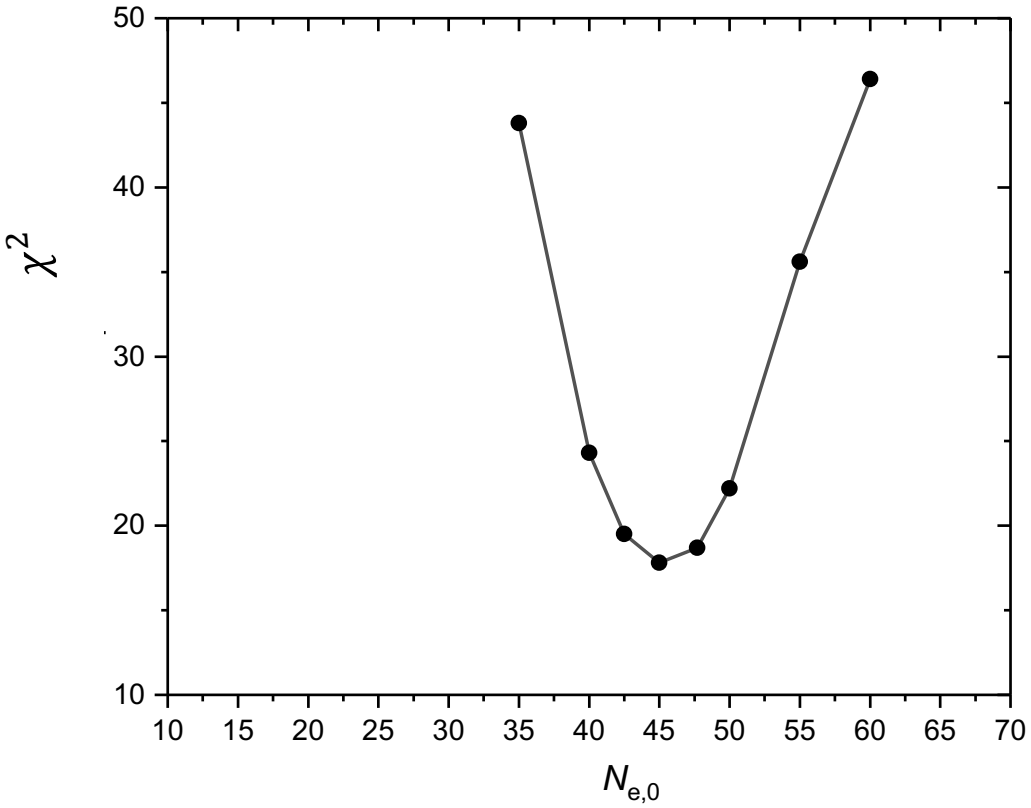

Fig. 5 χ^2 as a function of fixed values for $N_{e,0}$.

Within a few percent the fitted intensities agreed with expectation. For the monomer length l =0.568±0.012 nm was found in good agreement with $l = \sqrt{3C_\infty l_0^2}$ = 0.58 [31]. The results for ν are displayed in Table 1. Over the large range of N the exponent ν varies only very slightly and even for the largest ring with $N/N_{e,0} = 44$ the fractal dimension $d_f = \frac{1}{\nu} = 2.33$ is well below that of a mass fractal. Finally, we note that the fit is insensitive to the value of ν_{width}. For the fits displayed in Fig. 1 we imposed $\nu_{width} = 1$.

Inserting the fitted parameters and expanding Eqs. 10 with respect to Q^2, directly yields the radius of gyration R_g of the rings. The obtained results are included in Table 1 and displayed as a function of monomer number in a double logarithmic presentation in fig. 6. In terms of a power law description, the N -dependence of $R_g(N)$ is well accounted for by an exponent $\nu_{R_g} = 0.39 \pm 0.01$, smaller than the finding of $\nu = 0.43 \ldots 0.46$ for rings of M_n = 94 kg/mol and below, however, far away from mass fractal behavior. The error calculation both with respect to statistical as well as to systematic errors relating to linear contaminants are presented in Annex I.

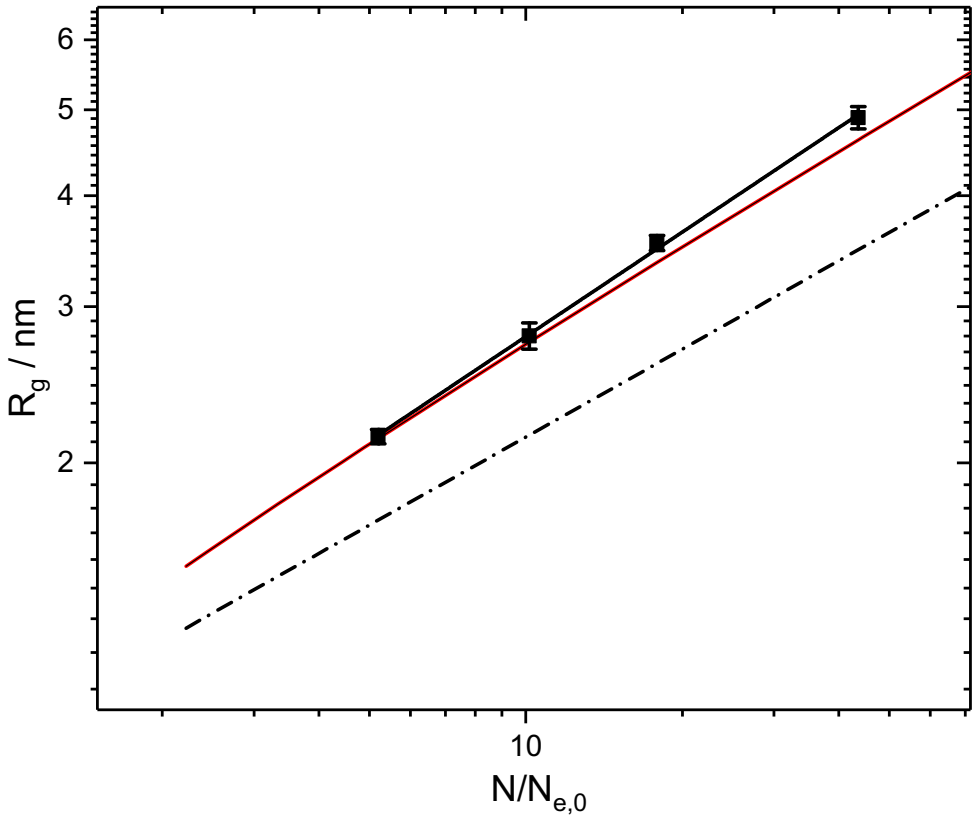

Fig. 6 Ring radii of gyration R_g as a function of ring size $N/N_{e,0}$. Solid black line: power law fit $R_g \sim (N/N_{e,0})^{\nu_{Rg}}$ with $\nu_{R_g} = 0.39 \pm 0.01$. Solid red line: prediction of Eq. 1 calculated on the basis of l = 0.568 nm and $N_{e,0}$ = 45. Dashed dotted black line indicates the mass fractal power law $R_g \sim \left(\frac{N}{N_{e,0}}\right)^{1/3}$. Copyright 2020 ACS

Discussion Ring Structure

The form factor of Eqs. 10 considers explicitly the ring structure as a self-similar object built from elementary Gaussian substructures and facilitates a nearly perfect and complete description of the SANS results; valid from the Gaussian substructures to the ring size for all molecular weights. The ring size independent cross over to $P(Q) \sim Q^{-2}$ is strong evidence for its interpretation as the experimental footprint of the elementary loops of size $N_{e,0}$. The different theories suggest that $N_{e,0}$ is to be expected close to N_e, the length of an entanglement strand in the corresponding linear melt. For PEO N_e has been determined by NSE on the scale of the reptation tube size resulting in $N_e = 59$ [24]. There the entanglement distance is directly derived from the topological confinement acting on the moving chain. From the plateau modulus in rheological measurements $N_e = 37$ is found [32]. This relatively large difference

is typical in the comparison of microscopic and macroscopic experiments and so far, is unresolved. $N_{e,0}$=45±2.5 is very close to the average between the two.

The exponent, describing the average distances within the ring (Eq. 9) depends very slowly on the ring size from ν=0.430 to ν=0.460 from N =1962 to N =234 again demonstrating that a ring with $N/N_{e,0} \cong 44$ is still far away from mass fractal statistics. The cross over from $\nu = \frac{1}{2}$ for the elementary loops to the smaller exponent in the self-similar regime appears to be relatively sharp, but the sensitivity of the fit towards the variation of the cross over width is weak. The existence of such a rather sharp cross over leads to a backlash of $r^2(|i-j|)$ in Eq. 9 at the cross over point again supporting the picture of elementary loops.

Having established experimentally the elementary loop size, we can check Obukhov's result for $R_g(N)$. Inserting $N_{e,0}$ into Eq. 1 $R_{e,0}^2 = \frac{l^2 N_{e,0}}{12} = 1.21\ \text{nm}^2$, the prediction of the decorated loop model is compared with the experimentally observed variation of R_g^2 with monomer number N - the agreement is nearly quantitative (fig.6). Note that the prediction of Eq. 1 is calculated solely on the basis of the experimentally determined values for l and $N_{e,0}$. We note, however, that the trend of R_g vs. $N/N_{e,0}$ appears to be slightly steeper than the Obukhov's prediction.

Opposing the predictions of other theories, in the decorated loop model the cross over to mass fractal behavior takes place only for very large rings. In terms of Eq. 1 a ring size in the order of $N/N_{e,0} > 10^4$ would be needed to reach this limit. This result also seems to disagree with some simulations that indicate a cross over to mass fractal behavior around $N/N_{e,0}$ about 10 - 15. [33]

Recently Halverson *et al.* [21] summarized all available results from simulations and presented them as shown in Fig. 7. There a properly normalized radius of gyration is plotted *vs.* $N/3N_e$. In this diagram on the small $N/3N_e$ side, where $R_g^2 \sim N$, the normalized radius of gyration squared increases with $N^{1/5}$. The onset of the asymptotic mass fractal behavior is characterized by a decrease of the normalized radius of gyration squared with $\left(\frac{N}{3N_e}\right)^{-2/15}$. In order to compare with our structural data, we normalized as $\frac{R_{g,\exp}^2(N)}{R_g^2(N_e,)(3N_e/N_e)^{0.78}\left(\frac{N}{3N_e}\right)^{4/5}}$; $R_{g,\exp}^2(N)$ denotes the experimentally observed radii of gyration from table 1, $N_e = N_{e,0} = 45$, $R_g^2(N_e) = 1.21\ \text{nm}^2$ and the exponent 0.78 relates to the experimentally observed power law

(Fig. 6). The magenta points present the results. As may be seen without any correction factors the simulation data follow very precisely the experimental results. As directly found by the measured N-dependence of R_g for the present $N/3N_e$values we are still not in the asymptotic mass fractal regime and again other than insinuated by Fig. 7 the cross over appears to be very broad.

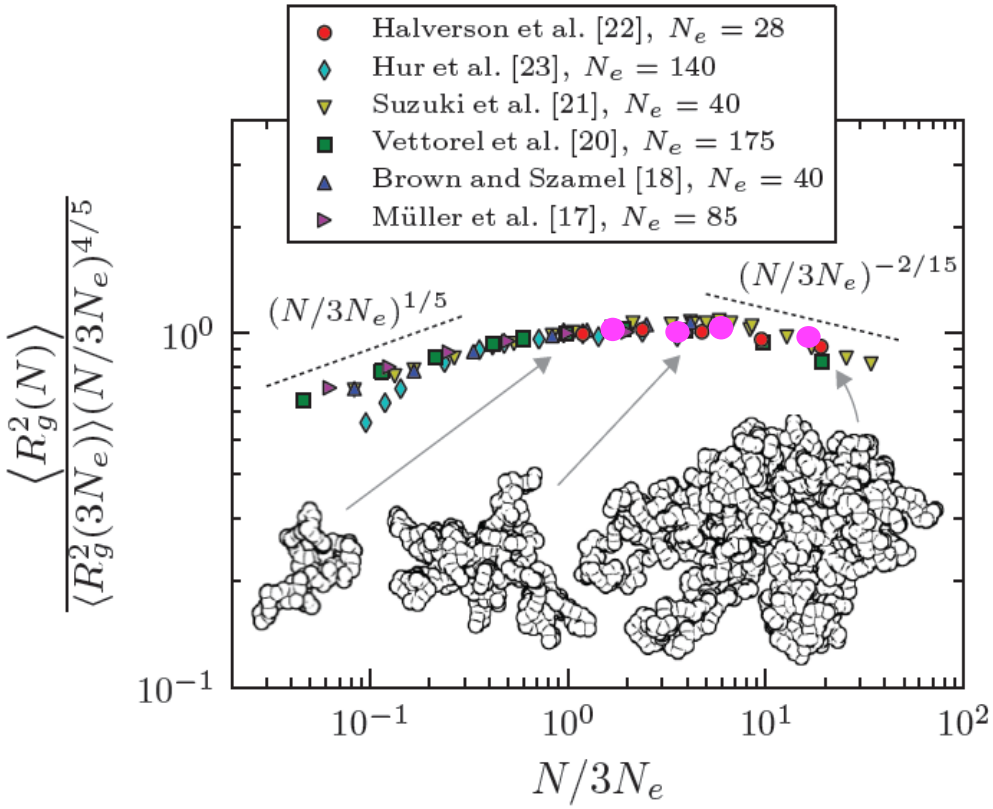

Fig. 7 Dependence of the ring $\langle R_g^2 \rangle$ on the reduced chain length [21]. For the references to the other simulation and experimental data see the original paper. Note, that $N_e = N_{e,0}$. The magenta points indicate the values obtained in this work. Copyright 2012 APS

Finally, a comparison with the results on PS-rings indicates that PS-rings are much closer to the structure of Gaussian rings even though a regime up to $N/N_{e,0} \cong 15$ was covered [9]. The large qualitative difference to the PEO-rings is difficult to rationalize. Perhaps the much larger inherent stiffness of PS compared to PEO plays a role. However, for generic

properties, as proposed in the different theories, one would not expect such different qualitative behavior.

Ring Dynamics

After structural characterization that established the existence of Gaussian substructures or elementary loops building the rings, we investigated the large scale dynamics of these rings. We addressed the long range diffusion for each ring applying pulse filed gradient NMR (PFG-NMR). Internal dynamics as well as the c.o.m. diffusion at the scale of the ring were investigated by NSE spectroscopy.

We performed the PFG-NMR measurements using a Varian 600 MHz system for the larger rings (R40, R100) and Minispec 20 MHz from Bruker for the smaller rings (R10, R20) at 413 K. The attenuation of the echo signal from a pulse sequence containing a magnetic field gradient pulse is used to measure the translational diffusion of the molecules (protons) in the sample at the time scale of tens of milliseconds. During this time the protons are able to overcome the distances of order of hundreds of nanometers. The diffusion coefficient was measured using a standard stimulated echo pulsed-field-gradient (STE) sequence [34]. The diffusion attenuation decay measured using STE sequence is determined by the equation:

$$A(\tau_1, \tau_2, g^2)/A(\tau_1, \tau_2, 0) = \exp\left(-\frac{\tau_2}{T_1}\right)\exp\left(-\frac{2\tau_1}{T_2}\right)\exp(-q^2(\Delta - \delta/3)D) \qquad (11)$$

where $q = g\gamma\delta$ is a generalized momentum transfer or scattering vector [35] with g and δ fixed to 5 ms being the magnetic field gradient strength and duration respectively and γ is the proton gyromagnetic ratio, τ_1 is the time interval between first and second radiofrequency pulses in STE sequence, τ_2 is the time interval between second and third radiofrequency pulses; T_1 and T_2 are the spin-lattice and spin-spin relaxation times respectively; Δ is the diffusion time set to 300 ms and D is the diffusion coefficient [35]. On definition $\Delta \approx \tau_1 + \tau_2$ and $\Delta \gg \delta$. It is worth to note, that Eq. 11 describes the diffusion spin echo decay of a monophase system obeying free Fickian diffusion behaviour. For all samples $\tau_2 \ll T_1$ and $\tau_1 \ll T_2$.

The diffusion attenuation decays are single exponential and exemplary presented in the Fig. 8.

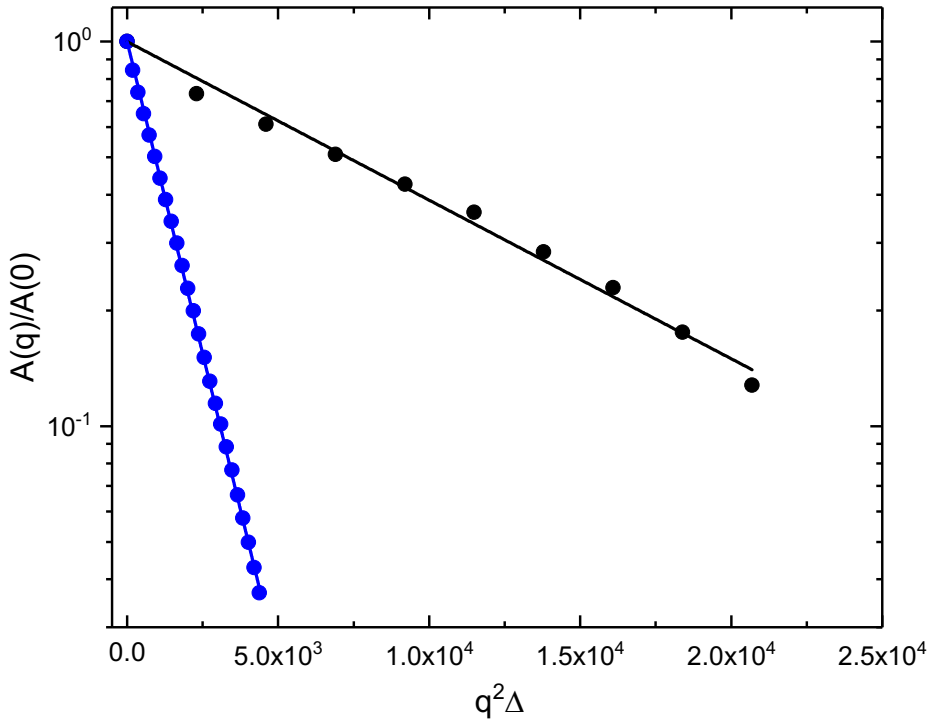

Fig. 8 PFG-NMR diffusion attenuation decays for the larger rings R40 (blue) and R100 (black). The solid lines are fitting to the Eq. 11.

The Fig 9 displays the NMR diffusion data at 413 K as a function of ring size in a double logarithmic plot revealing $D_{com}{\sim}N^{-2.2}$ in good agreement with Halverson's MD-simulations. Fig. 9 includes also diffusion data from linear PEO chains at 413 K. We find the slopes to be slightly different (-2.2 instead of -2.3) and the diffusivities differ by about a factor of 10 in reasonable agreement with simulations [25]. It has been found that the rings diffuse significantly faster than their linear counterparts. The authors try to explain this finding by the amoeba-like shape fluctuations, which do not require the complete reorganization of the internal winding of the ring chain. Very recently based on new microscopic dynamical theory Mei *et al.* [36] obtained $D_{com}{\sim}N^{-2}$.

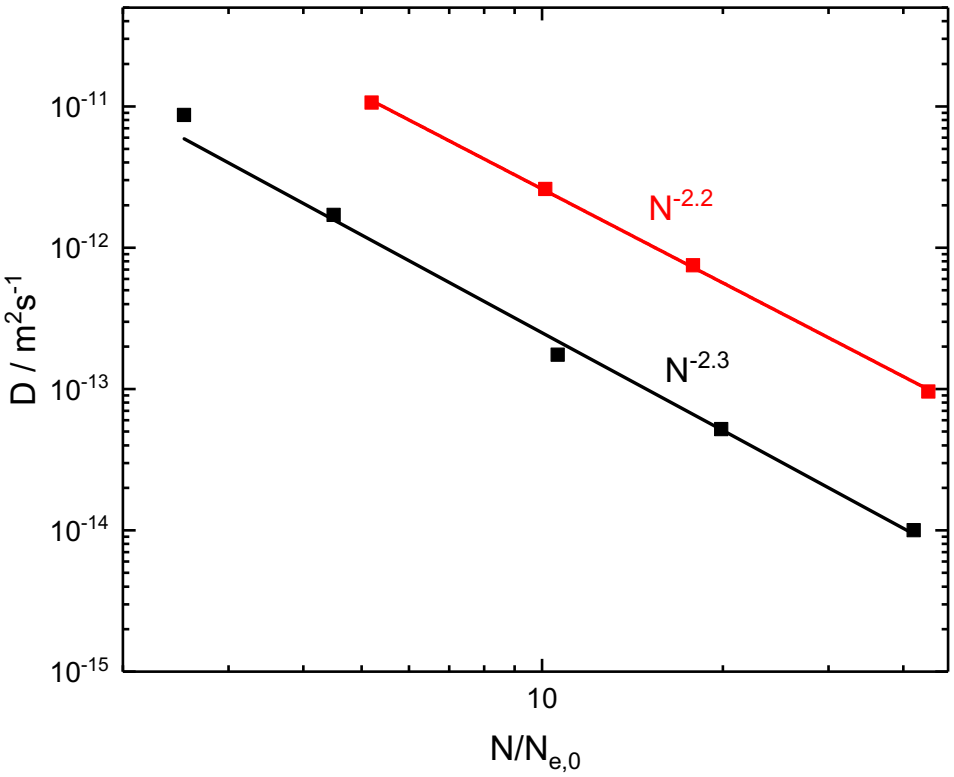

Fig. 9 PFG-NMR results for the diffusion constants for rings in the melt (red squares) as a function of chain length. Black squares show diffusion coefficients for corresponding linear PEO melts. Copyright 2020 APS

For the NSE experiments samples containing 10% protonated rings in the corresponding deuterated matrix were prepared. With these samples the NSE experiments addressed the intermediate dynamic structure factor $S(Q,t)$ related to the intra-ring dynamics. The measurements were performed at the instrument IN15 of the Institute Laue-Langevin in Grenoble, France. Using 3 different neutron wavelengths λ = 1.0, 1.35 and 1.7 nm a dynamic range $0.1 \leq t \leq 1000$ ns was achieved. The data were corrected for the scattering contribution of the deuterated matrix and the Niobium container. Fig 10 shows NSE-spectra from the two large rings, R40 and R100. The solid lines are the result of the theoretical description that will be discussed in the following.

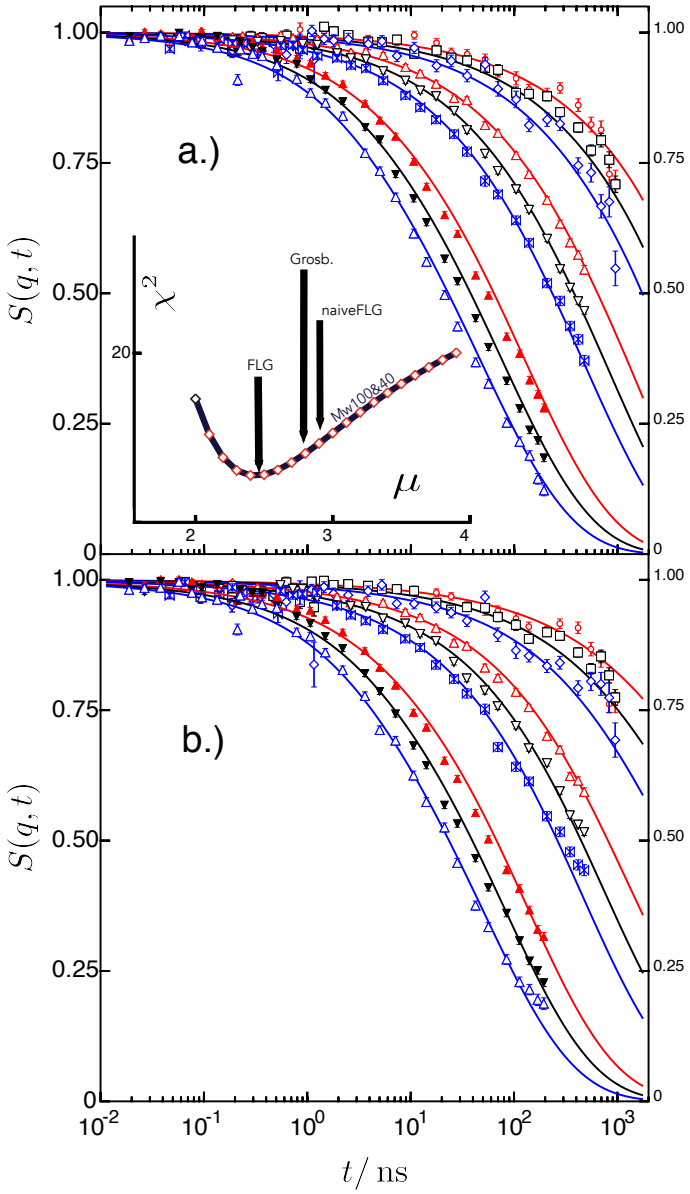

Fig. 10 NSE-spectra addressing the intra-ring pair correlation function (single chain dynamic structure factor) (a) from the R40 melt and b) from the R100 melt; the Q values from above are: 0.42, 0.49, 0.55, 0.69, 0.78, 0.86, 1.1, 1.2, 1.3 nm^{-1}. The solid lines represent the best fit using the scaling model (see text). The insert shows the sum of errors χ^2 revealed by a combined fit of NSE data for R40 and R100 as function of the spectral exponent μ. The arrows indicate the expectations from the discussed theory model. Copyright 2020 APS

The experiments aimed at scrutinizing the important elements of polymer ring dynamics. Requirements were: (i) The rings needed to be sufficiently large, in order to apply scaling approaches. (ii) The complex ring-dynamics demands to involve prior knowledge on the ring structure provided by SANS and the ring long range diffusion obtained by PFG-NMR.

The diffusion properties of polymer rings evidence three dynamic regimes, an early time sub-diffusive motion with $\langle r^2(t)\rangle_{com} \sim t^{\alpha}$ $(\alpha < 0.75)$ which is followed by the established $\langle r^2(t)\rangle_{com} \sim t^{3/4}$ dynamics [6,10] and finally by Fickian diffusion $\langle r^2(t)\rangle_{com} \sim D_0 t$. The first two regimes are accessible by NSE at least for the smaller rings, the long range Fickian diffusion D_0 by PFG-NMR. The c.o.m diffusion, respectively the corresponding dynamic structure factor $S(q,t) = \exp[-q^2/6\,\langle r_{com}^2(t)\rangle]$ reflects the time dependent c.o.m. mean-square-displacement $\langle r_{com}^2(t)\rangle$. The initial two-stage sublinear diffusion regimes are connected to the long-time Fickian diffusion D_0 by the following expression:

$$\langle r_{com}^2(t)\rangle = \left[\left(e^{\frac{1}{\beta}\left\{(-\alpha+\beta)\ln\left(\frac{\langle r_1^2\rangle}{\langle r_2^2\rangle}\right)+\beta\alpha\left[-ln\left(\frac{\langle r_2^2\rangle}{6D_0}\right)\right]\right\}}\langle r_2^2\rangle t^{\alpha}\right)^{a} + \left(e^{\left\{-\ln\left(\frac{\langle r_2^2\rangle}{6D_0}\right)\right\}\beta}\langle r_2^2\rangle t^{\beta}\right)^{a} + (6D_0 t)^{a}\right]^{1/a} \quad (12)$$

It describes the transition from an initial sub-linear diffusion with a MSD $\propto t^{\alpha}$ until a MSD-value of $\langle r_{\mathrm{com}}^2(t)\rangle = \langle r_1^2\rangle$ is reached; then the c.o.m diffusion crosses over to MSD $\propto t^{\beta}$ until a MSD of $\langle r_{\mathrm{com}}^2(t)\rangle = \langle r_2^2\rangle$ is reached, where finally normal Fickian diffusion with a diffusion coefficient D_0 sets in. The sharpness of the transitions is controlled by a, the larger the value the sharper is the transition. Further Eq. 12 assumed that $0 < \alpha < \beta < 1$ and $\langle r_1^2\rangle < \langle r_2^2\rangle$. The explicit form of Eq. 12 follows from the requirement that the input parameters for this phenomenological description are the long time diffusion D_0, the two sub-linearity exponents α and β and the MSD values $\langle r_1^2\rangle$ and $\langle r_2^2\rangle$ that separate the regimes. The transition times at these MSD's and the continuity of $\langle r_{\mathrm{com}}^2(t)\rangle$ between the regimes is ensured by the form of Eq. 12.

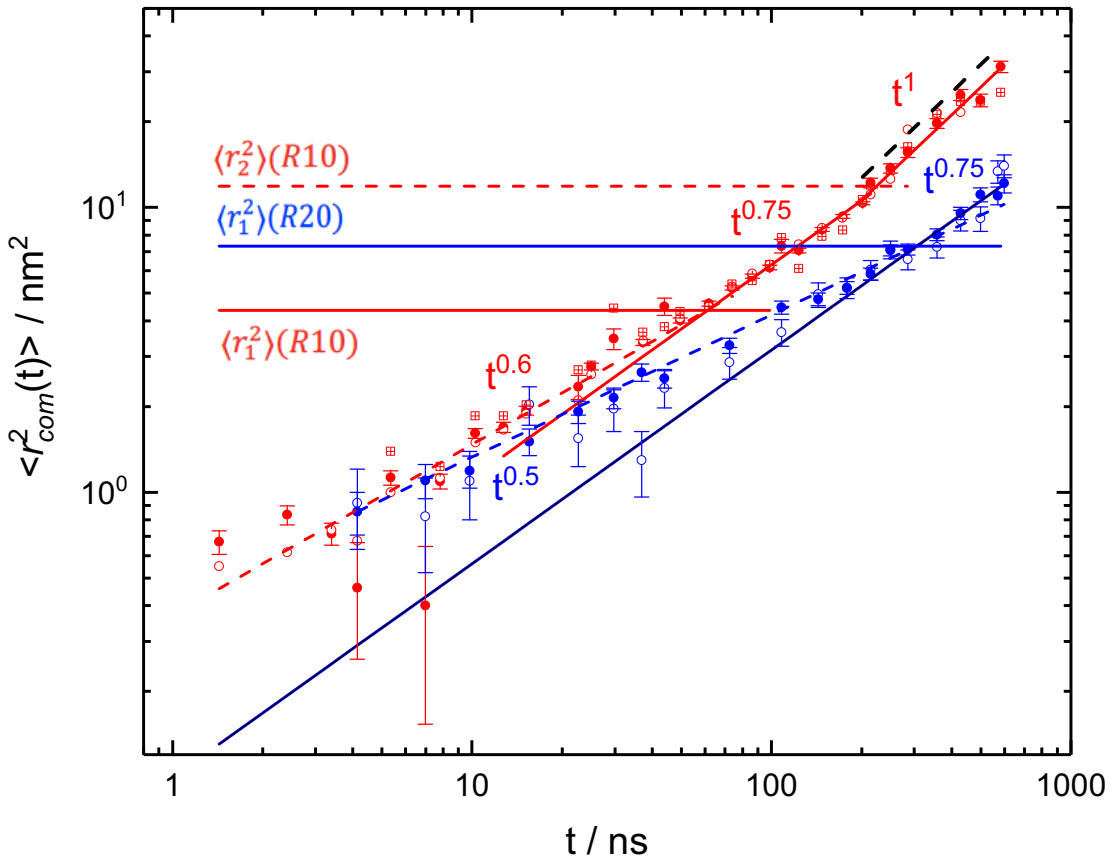

Fig. 11 Center of mass MSD as evaluated directly from the dynamic structure factor (see text) for R10 (red) and R20 (blue). Red crossed squares, open and filled circles correspond to $Q = 0.3, 0.5$ and $0.8\ \mathrm{nm}^{-1}$ for R10; blue filled and open circles relate to $Q = 0.3, 0.5\ \mathrm{nm}^{-1}$ for R20. The horizontal lines mark the different cross-overs $\langle r_1^2\rangle$ and $\langle r_2^2\rangle$. Dashed black line shows the MSD extrapolated from PFG-NMR diffusivity measured for R10 ring. Copyright 2020 APS

Fig. 11 displays the $\langle r_{com}^2(t)\rangle$ for R10 and R20 that are directly derived from the structure factor as $\langle r_{com}^2(t)\rangle = -6/Q^2 \ln[S(Q,t)]$ taken at sufficiently low Q, such that internal modes do not contribute (R10: Q = 0.3, 0.5, 0.8 nm^{-1}; R20: Q = 0.3, 0.5 nm^{-1}). The R10 $\langle r_{com}^2(t)\rangle$ clearly displays two cross-overs at $\langle r_1^2\rangle \cong 4.4\ \mathrm{nm}^2$ and $\langle r_2^2\rangle \cong 12.0\ \mathrm{nm}^2$, while for R20 only the first cross over $\langle r_1^2\rangle \cong 7.4\ \mathrm{nm}^2$ is visible. The cross-overs are marked by horizontal lines in Fig. 11. From simulations we know that $\langle r_2^2\rangle$ is expected to take place around $\langle r_2^2\rangle \cong 2 \ldots 3\ R_g^2$. For R10 we have $\langle r_2^2\rangle / R_g^2 = 2.6$ in very good agreement with simulations. The first cross over $\langle r_1^2\rangle$ was already found earlier but remained unexplained [10]. We find $\langle r_1^2(20K)\rangle / \langle r_1^2(10K)\rangle$=1.68 very close to the ratio of the two radii of gyration $2.78^2/2.14^2 = 1.69$ (see Table 1) leading us to conjecture that $\langle r_1^2\rangle$ relates to the correlation hole effect as proposed for linear polymers by Guenza [37] that scales with R_g and leads to

c.o.m sub-diffusivity characterized by an exponent α. For linear chains α decreases with increasing molecular weight [38]. With these results we then scale $\langle r_1^2 \rangle$ and $\langle r_2^2 \rangle$ toward higher M_n as $\langle r_1^2 \rangle, \langle r_2^2 \rangle \sim R_g^2 \sim N^{0.78}$ (see Fig. 6). The long range Fickian diffusion D_0 was taken from PFG-NMR and corrected for the NSE temperature.

The internal ring motions are considered to evolve in two steps: At short time and distances the elementary loops perform Rouse dynamics with mode relaxation times $\tau_p \sim p^{-2}$, where p is the mode number. For larger distances and times the regime of loop relaxation follows. In terms of scaling theories, there the mode spectrum has the form $\tau_p = \tau_2 p^{-\mu}$, where τ_2 is the first ring mode (only even modes are allowed) and μ the scaling exponent. Via a continuity condition at τ_e the two regimes are connected. The dynamic structure factor for the internal ring dynamics assumes the form:

$$S_{int}(Q,t) = \frac{1}{N}\sum_{i,j}^{N} \exp\left[\frac{(Ql)^2}{6}\left(\frac{|i-j|\{N-|i-j|\}}{N}\right)^{2\nu(|i-j|)} - B_{i,j}(t)\right] \qquad (13a)$$

with

$$B_{i,j}(t) = 2N^{2\nu(|i-j|)}(lQ)^2/(3\pi^2)\sum_{p,even}\frac{1}{p^2}\cos\left(\frac{p\pi[i-j]}{N}\right)\left[1-\exp\left(-t\Gamma(p)\right)\right] \qquad (13b)$$

$\nu(|i-j|)$ delineates the conformational cross over from Gaussian statistics at distances $|i-j| \le N_{e,0}$ to compressed behavior $|i-j|^{\nu}$ at larger distances. It is described by Fermi-type cross over functions taken from the SANS-results: $\nu(n) = T_n(n)\nu + \left(1-T_n(n)\right)\nu_1; \nu_1 = 1/2$ with $T_n(n) = \{1+\exp[(n-n_{trans})/n_{width}]\}^{-1}$, where $n_{trans} = N_{e,0}$. For the relaxation rate

$$\Gamma(p) = \frac{\left[1-T_f(p)\right]\pi^2 W l^4 p^2}{N^2 l^4} + T_f(p) W \pi^2 \left(\frac{p}{p_{min}}\right)^{\mu} (p_{min}/N)^2 \qquad (14)$$

holds. $T_f(p) = \{1+\exp[(p-p_{min})/p_{width}]\}^{-1}$ is the cross over function in p with p_{min} the number of elementary loops $p_{min} = N/N_{e,0}$ within the ring. From SANS $N_{e,0} = 45$, revealing p_{min} = 5, 10, 22, 44 for our rings and μ the spectral exponent. The basic Rouse rate $Wl^4 = 1.489$ nm^4/ns is taken from NSE experiments on M_n=190 kg/mol PEO melts also measured at the same temperature [24]. Including all prior knowledge, we jointly fitted the spectra resulting from R40 and R100 varying only the spectral exponent μ and the exponents α_{R40} and α_{R100} that describe the first sub-diffusive regime of the c.o.m diffusion [37]. All other

parameters remained fixed. Since the fits did not depend much on p_{width}, in order to establish a smooth cross over, we chose $p_{width} = 0.1 p_{min}$. As Fig. 11 demonstrates the model leads to an excellent fit of all the spectra. For the slopes α in the first sub-diffusive regime we obtain: $\alpha_{R10} = 0.65$; $\alpha_{R20} = 0.53$; $\alpha_{R40} = 0.54$ and $\alpha_{R100} = 0.41$. Similar small exponents for the initial diffusion regime were also reported in recent MD-simulations for PE-rings [27]. For the scaling exponent the joint fit reveals $\mu = 2.4 \pm 0.1$. We note that the fit results are very sensitive to the fractal exponents ν, thus it is essential to fix them to the values, which were obtained with high precision by SANS (better than 1%). Applying the same fitting procedure also to the large Q-regime of the R10 and R20 rings, we find μ(R10)=5.0 and μ(R20)=2.66; seemingly these smaller rings are not yet large enough to apply scaling considerations. Fig. 12 displays the best fits to the ring samples with lower (nominal) $M_n = 10$ and 20 kg/mol that are marginal or well below the scaling regime. Figs. 12 (a,b) show that also for these rings the model expression (Eq. 13) matches the NSE data nearly perfectly with just two free fitted parameters α and μ.

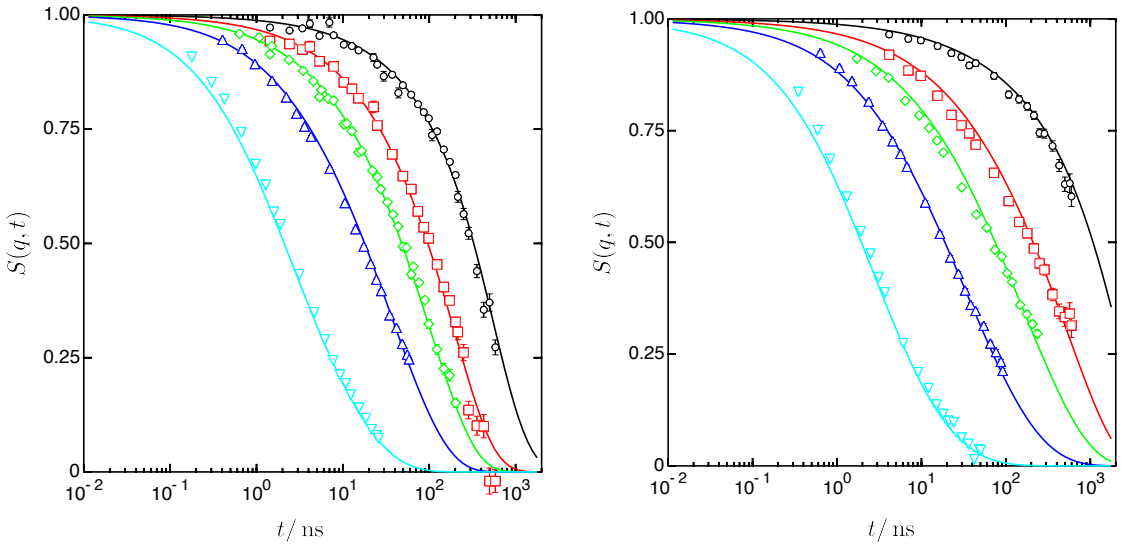

Fig. 12 Fits of Eq. 13 to the ring R10 (a); and to the ring R20 (b). The Q-values from right to left were 0.5, 0.8, 1.0, 1.3, 2.0 nm^{-1} . Data taken from Gooßen *et al.* [10]

Discussion Ring Dynamics

Discussing the results, we first emphasize the overall goodness of fit: With only 3 fit parameters all spectra are excellently described. Let us now turn to the diffusion properties. The data analysis confirmed the 3 dynamic regimes of center off mass diffusion. In particular

the physical origin of the of the novel early time regime seems to be clarified. Showing several attributes of the short time diffusion of linear chains in the melt, we conjecture that it results as a consequence of the correlation hole potential as first suggested by Guenza for linear chains: (i) Its dynamic regime extends to a range comparable to R_g^2 and it scales with R_g^2. This can be directly read off from the R10 and R20 $\langle r_{com}^2(t)\rangle$ and is corroborated by the excellent fits for R40 and R100; (ii) the exponents α decrease with increasing M_n, as was observed for linear PE melts [38]. On the basis of polymer integral equation theory recently Dell and Schweizer also emphasized the importance of correlation hole effects [39]. The M_w dependence of $D{\sim}N^{-2.2}$ agrees well with large scale MD-simulations but disagrees with all the scaling models that predict diffusion exponents between about -1.6 (FLG) and -2 (DFLA, naive FLG). Seemingly the simple scaling argument $D{\sim}R_g^2/\tau_d{\sim}N^{0.78}/N^{2.4}{\sim}N^{-1.62}$ does not hold. In considering important caging effect (see also Ref. [40]) the theory of Mei *et al.* finds that $\tau_d{\sim}N^{8/3}$ and $D{\sim}N^{-2}$, so $D{\sim}R_g^2/\tau_d$ is reasonable zero order approximation since the theory analysis [11] employed $R_g{\sim}N^{1/3}$ as a simple model. Nevertheless, for a finite ring our data are not in accordance with such a prediction ($D{\sim}N^{-2.2}$; $\tau_d{\sim}N^{2.4}$ and $R_g{\sim}N^{0.39}$ that results in $\frac{R_g^2}{\tau_d}{\sim}\frac{N^{0.78}}{N^{2.2}}=N^{-1.64}\neq N^{-2.2}$).

Using a microscopic theory for time-dependent sub-diffusive c.o.m. motion Mei *et al.* [36] demonstrated that the sub-linearity exponent over broad length and time interval is a distance and time-dependent. This is in qualitative agreement with our results ($0<\alpha<\beta<1$). However, if try to make a quantitative comparison, we realize that the experimental exponents are systematically smaller than those predicted by theory. For the R20 ring, where we directly measured the time dependent c.o.m MSD, we are in the regime of normalized $\tilde{R}(t)=\sqrt{\langle r_{com}^2(t)\rangle/R_g^2}$ between 0.31 and 1.3. The R20 ring is built from N=445 monomers. If we compare with the prediction of Fig. 8 in Ref. [36] we should find values of γ between 0.8 and 0.95. We actually observe a short time slope $\alpha=0.6$ that around $t=300$ ns crosses over to $\alpha=0.75$. Thus, a quantitative comparison with the theory by Mei *et al.* fails. This also holds, if we compare with the calculations for the next smaller N=200 or larger N=800 cases. For our R100 ring, where we inferred the c.o.m. MSD from the fit, the exponent came out as $\alpha=0.41$ in contrast to the theory predictions that lie in between 0.55 and nearly 1.

The concept of internal motion that takes place within two different dynamic regimes is well supported by our data. As the ring conformations already show, at short distances along the chain $|i-j| \leq N_{e,0} = 45$ the conformation is Gaussian and like in linear polymers Rouse dynamics is a valid model. Beyond this limit the conformation is compressed and loop dynamics is proposed theoretically - the different scaling models distinguish themselves by different spectral exponents. The quality of the data description (i) shows that scaling models are well supported and (ii) the scaling exponent μ comes out close to the FLG prediction. In order to get an impression how significant the extracted value for the spectral index μ is, in the insert of Fig. 10a we plot the sum of residual errors χ^2 obtained by comparison of values of $S(q,t)$ from the model and the NSE data from R40 and R100 simultaneously for all available Q-values. For each preset value of μ the two slightly different α values for R40 and R100 were allowed to vary to find the minimum of χ^2 fit.

Note that the ideal value of $\chi^2 = 1$ for a best fit is not reached due the fact that the pure statistical errors of the NSE data are quite small such that they are of the same order of magnitude or below residual systematic fluctuation of the data points due to external magnetic noise or other stability issues and residual imperfections of the model functions. However, the matching shown in the figures reveals that the fitting quality is still extraordinarily good over the whole accessed time and wavevector range for a model with only two fitting parameters μ, α. As discussed above, the exponent α characterizing shorter time scale sub-diffusive behavior depends on the molecular weight (see Table 1). Mei *et al.* [36] also addressed this point showing that the minimum of the temporal γ exponent becomes deeper with increasing N and called it an open problem. This fact is not captured by the scaling models. However, as we state above, correlation hole effects could be a means to describe this phenomenon.

To put the value of μ in the context of ring size effects and further estimate its error the following considerations can be made. If we take the analogy to phase transitions, then finite size effects may arise from the distance of the actual ring size from the ideally large ring that displays mass fractal behavior. In table 1 we have quoted the effective scaling exponents that arise for rings with fractal dimensions as observed by SANS. E.g. for the R100 ring we found $d_f = \frac{1}{\nu} = 2.33$ rather far apart from the asymptotic large N value of $d_f = 3$. Consequently, the exponent for $\tau_p = \tau_e \left[N/N_{e,0}\right]^{\left(2+\frac{1}{d_f}\right)=\mu}$ changes from $\mu = 2.33$ for $d_f = 3$ to $\mu = 2 + \frac{1}{2.33} = 2.43$ because of the finite ring size. Similarly, the other exponents are affected. From another side we might look at the values we obtain for smaller rings: As quoted above for R10 $\mu = 5.0$ and for R20 $\mu = 2.66$ arise, while a joint fit of R40 and R100 reveals $\mu = 2.4$. Thus, the

exponents show the tendency to decrease with increasing ring size.

As Fig. 12 shows, the theoretical curves fit extraordinary well the experimental data. Consequently, the fit results in very small statistical errors on the order 1%. Systematic errors are very difficult to estimate, but from comparing results that were obtained by varying the many input parameters within their statistical accuracies, we came to the conclusion that the uncertainty of μ is on the order of 0.1. Nevertheless, our experiments agree best with Rubinstein's self-consistent FLG model [11] for the internal ring dynamics even though the predictions for diffusion are not fulfilled.

The segmental MSD may be directly studied by incoherent neutron scattering, which measures the self-correlation function of the protons. In this case the structure factor arising from the self-correlation-function has the form:

$$S_{self}(Q,t) = \mathrm{A}(Q)\,\exp\left[-\frac{Q^2}{6}\langle r^2(t)\rangle\right] \qquad (15)$$

where $\langle r^2(t)\rangle$ is the average MSD of a monomer containing both motion by intra chain relaxation as well by translational c.o.m. diffusion, $\mathrm{A}(Q)$ is the Debye-Waller factor. There are some disadvantages as well as virtues of using a conventional NSE spectrometer for the spectroscopy of spin-incoherent scattering. First of all, NSE is the only neutron spectroscopic method with high enough time/energy resolution in the relevant Q range. However, there is an inherent penalty due to the fact that the spin of the scattered neutron is flipped with a probability of 2/3. Therefore, the remaining net polarization is -1/3 of the original yielding a sign reversed reduced echo signal on an additional background amounting to 2/3 of the total scattering. A virtue of the spin-flip scattering is that multiple scattering is efficiently suppressed since two subsequent scattering events only leave 1/9 of the signal and higher level multiple scattering events contribute even less to the spin echo amplitude. The overall intensity is much smaller (10 . . . 20 times) than the coherent small angle scattering from chain labeled samples. Because of the low scattering intensity very careful background measurements from the sample container and spectrometer components are necessary.

Employing the NSE instrument IN15 at the ILL, using neutrons with $\lambda = 0.6$ nm we studied $S_{self}(Q,t)$ for the ring hR100 and the corresponding linear chain hL100 (see table 1). The samples had a transmission of 60%. Fig. 13 displays the measured spectra after background subtraction for both materials at $Q = 1.2$ nm^{-1} and $Q = 1.7$ nm^{-1}. We note that at early times the spectra from the ring and the linear polymer are nearly identical, while at longer times the ring polymer relaxes somewhat faster than the linear chain. A reliable MSD may only be evaluated from spectra that have not decayed too much ($S(Q,t)/S(Q,0) \geq 0.05$). Thus, in order to cover long times the corresponding Q-value needs to be as small as possible. As it

turned out for $Q < 1.2$ nm^{-1} the coherent background from the sample container and instrument components was too large to allow a meaningful data evaluation. This restricted the time range to $t_{max} = 40$ ns.

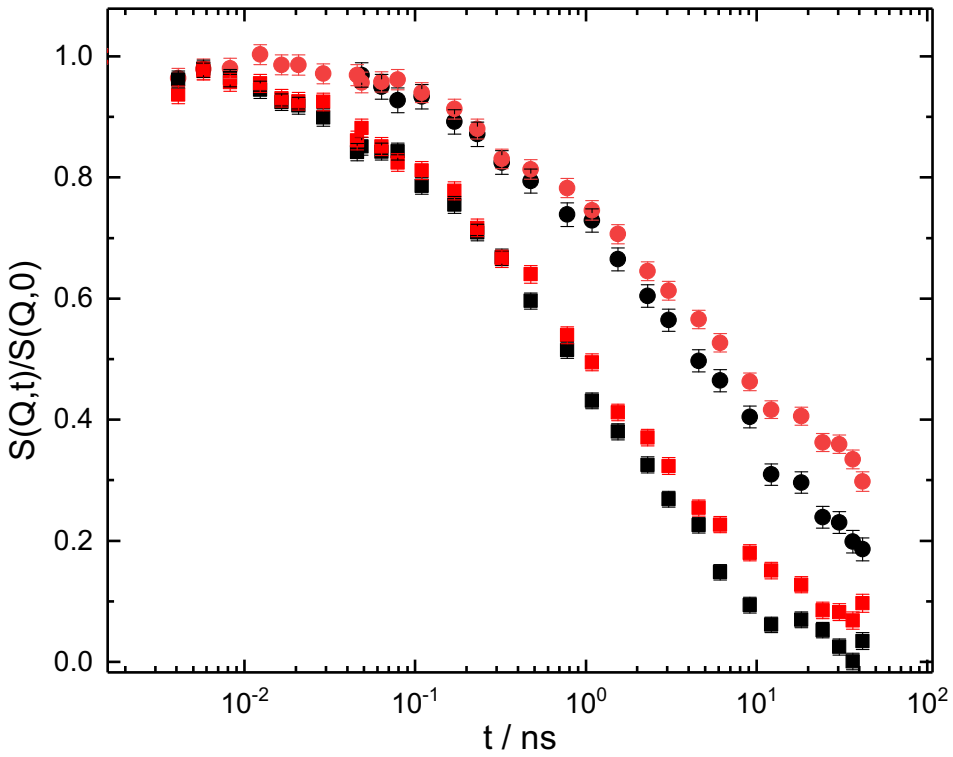

Fig. 13 Incoherent spectra from the linear polymer hL100 and the ring R100 at Q-values of $Q = 1.2$ nm^{-1} (circles) and $Q = 1.7$ nm^{-1} (squares).

From these spectra at $Q = 1.2$ nm^{-1} and 1.7 nm^{-1} the segmental MSD were directly determined using $\langle r^2(t)\rangle = -{}^{6}/_{Q^2} \ln\left(S_{self}(Q,t)/S_{self}(Q,0)\right)$. For both the linear as well as the ring polymer the results are displayed in Fig. 14 in a double logarithmic plot.

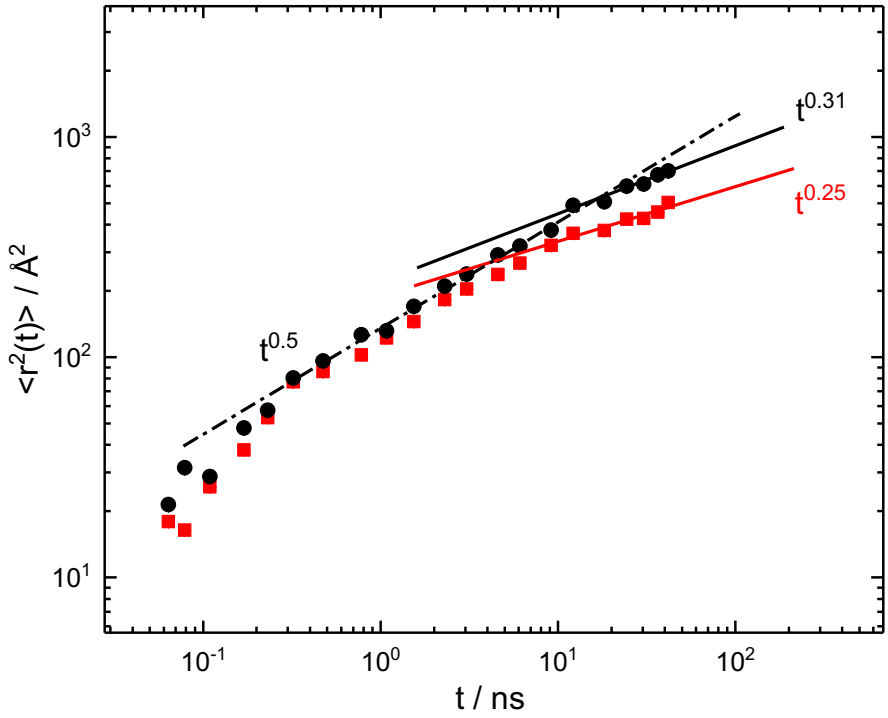

Fig. 14 Segmental MSD derived from the incoherent spectra of hL100 (red squares) and hR100 (black dots) in a double logarithmic presentation. The lines display the limiting power laws for Rouse motion ($t^{1/2}$) and local reptation ($t^{1/4}$) and an empirical power law for rings [10,25].

As predicted by the Rouse model initially at shorter times the MSD of both polymers nicely follow a $t^{1/2}$ power law. As a consequence of the comparatively very small translational diffusion of the linear chain its MSD comes out slightly below that of the ring, where the translational diffusion matters (see Fig. 14). Then for the linear chain at a cross over time $\tau_e^{self} \cong 8$ ns the time - power law weakens and changes to time dependence compatible with $t^{1/4}$ power law, which is expected for local reptation. Compared to the expected $\tau_e = \frac{d^4}{\pi^2 W l^4} =$ 33 ns the cross over time observed in the self-correlation function is shorter by about a factor of 4 [40]. This relates to the different type of physical effect that underlies the segmental MSD being affected by tube constraints: Whenever on average a segment pervades half of the tube size the tube constraints affects its motion. On the other hand, the coherent signal stems from chain fluctuations probing the lateral constraints. While for the linear chain the cross over to local reptation is evident, for the ring the relative slowing down of the MSD appears to be somewhat less pronounced and takes place at somewhat later time (13.5 ns).

Finally, Fig. 15 displays the results from the hydrogenated hR100 in the context of the overall picture of ring dynamics, as it was derived on the basis of the coherent scattering

explained above. Using the model parameters obtained from the spectral fit (Fig. 10) we calculated the predictions for the MSD due to translational and internal motion reaching out to the regime of Fickian diffusion at times beyond in the order of 10^6 ns. The red dashed dotted line presents the segmental MSD, while the green sold line marks the c.o.m. MSD. Both add to the solid blue line describing the total MSD of a segment that is observed by the incoherent experiment. It is very satisfying to find the excellent agreement between the data for the self-correlation function obtained in an independent experiment with the prediction on the basis of the coherent scattering data underlining the consistency of the data evaluation.

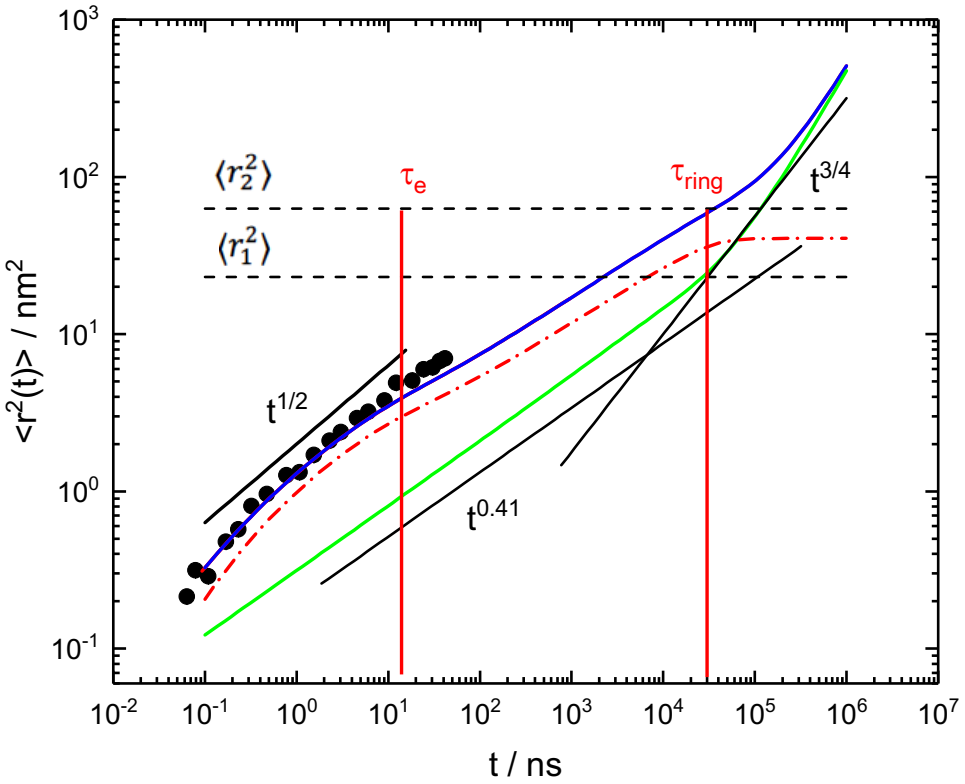

Fig. 15 Comparison of the segmental MSD for R100 ring, directly obtained from the self-correlation function (incoherent scattering) (symbols). Solid blue line presents MSD calculated from the best fit of the pair correlation function (Eqs. 13). Dash horizontal lines show the $\langle r_1^2 \rangle$ and $\langle r_2^2 \rangle$. The solid green line represents the c.o.m MSD as fitted with our model (for the exponent see Table 1) and red dash-dotted line is the segmental MSD. The black solid lines demonstrate power laws, the vertical lines τ_e, τ_{ring} indicate the loop Rouse time and longest relaxation time of the ring, respectively. The figure extends the time range showing the predicted full dynamic regime based on the obtained fit parameters. Copyright 2020 APS

Conclusion

We have presented a comprehensive study on the structure and dynamics of very large well defined ring polymers and were able to scrutinize existing theories and large scale simulations. The evaluation of ring conformations in the melt established

- the existence of Gaussian substructures with a size that is independent of the ring molecular weight. We have associated these substructures with the predicted elementary loops of a dimension close to the entanglement length of their linear counterpart.
- the overall ring dimensions follow a power law as a function of the monomer number. The magnitude of R_g^2 quantitively agrees with a compilation of simulation results [21]. However, other than suggested on the basis of these simulations, the experimentally determined power law exponent for R_g of $\nu_{R_g} = 0.39$ shows that the mass fractal regime is not yet reached ($\nu = 0.33$).
- Yet, the dependence of R_g on N agrees very well with the predictions of Obukhov's decorated loop model [17].

The long range ring diffusion was investigated by PFG-NMR. Internal relaxation and short time c.o.m. diffusion was studied by neutron spin echo spectroscopy. The following results stand out:

- Long range Fickian diffusion of rings in their melt follows a power law $D \sim 1/N^{2.2}$ in good agreement with simulations but contradicting scaling theories that all predict exponents ≤ 2 and also recent theoretical predictions of an exponent of 2. The magnitude of the diffusion coefficients is a bout 10 times smaller than that of the corresponding linear melt again in rather good agreement with simulations.
- Center of mass diffusion on the scale of the molecule is characterized by two subsequent power laws in t; starting with $\langle r_{com}^2(t)\rangle \sim t^{\alpha}$ until the MSD reaches a magnitude $\cong R_g^2$ then crossing over to $\langle r_{com}^2(t)\rangle \sim t^{\beta}$ with $\alpha < \beta = 3/4$. While the second power law has been predicted theoretically, the first power law displays striking similarities to conclusions based on the correlation hole effect [36].
- For the internal relaxation of rings a number of different scaling theories exist that for loops larger than the elementary loop predict different spectral exponents for the dependence of the relaxation time on the mode number p: $\tau_p \sim p^{-\mu}$. The NSE result of $\mu = 2.4 \pm 0.1$ favors the Fractal Loopy Globule model by Rubinstein *et al.* [11]

- Finally, we have directly measured the segmental MSD, that perfectly agrees with what is calculated by the model describing the single chain dynamic structure factor underlining the internal consistency of our approach.

With this work we present a combined study both on the ring conformation as well as on their dynamics taken on the same very large rings, where finite size effects should be weak. The results may serve as a benchmark for the development of a better theoretical understanding of these topologically unique polymers.

Appendix I

The errors in R_g were obtained by evaluating the sum of errors taken at one σ statistical deviation of the two relevant fit parameters monomer length l and fractal exponent $\nu = 1/d_f$ determining R_g. Table AI represents the detailed results.

Table A1 Radii of gyration R_g calculated at the one sigma statistical deviation of the fractal exponent $\nu = 1/d_f$ and the monomer length l

Ring	$R_g[nm]$	l $[nm]$	$R_g(l+\Delta l)$ $[nm]$	$R_g(l-\Delta l)$ $[nm]$	ν	$R_g(\nu+\Delta\nu)$ $[nm]$	$R_g(\nu-\Delta\nu)$ $[nm]$
R100	4.94	0.583±0.012	5.04	4.84	0.433±0.003	50.25	48.5
R40	3.56	0.561±0.012	3.63	3.48	0.448±0.003	36.0	35.0
R20	2.88	0.573±0.012	2.93	2.81	0.451±0.010	3.00	2.76
R10	2.17	0.555±0.012	2.21	2.11	0.460±0.003	2.18	2.14

The final errors were calculated from the sum of errors:

$$\Delta R_g = \sqrt{\frac{1}{2}\left[\left(R_g(l) - \overline{R_g(l \pm \Delta l)}\right)^2 + \left(R_g(\nu) - \overline{R_g(\nu \pm \Delta\nu)}\right)^2\right]} \qquad \text{(A1)}$$

Furthermore, linear contaminants may influence the apparent R_g. Scattering observes the z-average of the radii of gyration. The narrow molecular weight distribution does not result in any important correction. However, the admixture of linear contaminants needs to be scrutinized. The z-average is calculated as

$$\langle R_g^2 \rangle_z = \frac{\sum w_i M_i \langle R_g^2 \rangle_i}{\sum w_i M_i} \tag{A2}$$

where w_i are the mass fractions and M_i the component masses. Since the masses of the ring and the leading linear contaminant are equal Eq. A2 reduces to

$$\langle R_g^2 \rangle_z = \frac{\sum w_i \langle R_g^2 \rangle_i}{\sum w_i} \tag{A3}$$

With the size of the linear component $\langle R_g^2 \rangle_{lin} = \frac{1}{6} l^2 N$ we may equate Eq. 12 to:

$$\langle R_g^2 \rangle_{ring} = \frac{\langle R_g^2 \rangle_{observed} - w_{lin} \langle R_g^2 \rangle_{lin}}{w_{ring}} \tag{A4}$$

With the linear weight fractions obtained from characterization, table A1 presents the corrections.

Table A2 Corrections for the radii of gyration as a consequence of linear contaminants

Ring	w_{lin}	Correction ΔR_g^{ring} [nm]
R100	below 1%	less than -0.08
R40	below 1%	less than -0.04
R20	3.5%	- 0.1
R10	1.5%	- 0.03

For the two largest rings the correction will be smaller than the quoted values. The exact amount cannot be given since the linear contamination came out to be smaller than 1%. We estimate that half of the quoted value is the true value. In Table A1 we have corrected for half of ΔR_g^{ring} and added the other half to the uncertainty.

References

[1] M. Kruteva, J. Allgaier, M. Monkenbusch, L. Porcar, and D. Richter, ACS Macro Lett. **9**, 507 (2020).

[2] M. Kruteva, M. Monkenbusch, J. Allgaier, O. Holderer, S. Pasini, I. Hoffman, and D. Richter, Phys. Rev. Lett. **125**, 238004 (2020).

[3] M. Doi and S.F.Edwards, *The Theory of Polymer Dynamics* (Clarendon press Oxford, Oxford, 1986).

[4] J. Anthony Semlyen, editor , *Cyclic Polymers* (Kluwer Academic Publishers, 2002).

[5] D. Richter, M. Monkenbusch, A. Arbe, and J. Colmenero, *Neutron Spin Echo in Polymer Systems* (Springer Berlin Heidelberg, Berlin, Heidelberg, 2005).

[6] D. Richter, S. Gooßen, and A. Wischnewski, Soft Matter **11**, 8535 (2015).

[7] P. G. De Gennes, *Scaling Concepts in Polymer Physics* (Cornell University Press, 1979).

[8] T. Cremer and C. Cremer, Nat. Rev. Genet. **2**, 292 (2001).

[9] T. Iwamoto, Y. Doi, K. Kinoshita, Y. Ohta, A. Takano, Y. Takahashi, M. Nagao, and Y. Matsushita, Macromolecules **51**, 1539 (2018).

[10] S. Gooßen, A. R. Brás, M. Krutyeva, M. Sharp, P. Falus, A. Feoktystov, U. Gasser, W. Pyckhout-Hintzen, A. Wischnewski, and D. Richter, Phys. Rev. Lett. **113**, 168302 (2014).

[11] T. Ge, S. Panyukov, and M. Rubinstein, Macromolecules **49**, 708 (2016).

[12] P. G. de Gennes, J. Phys. Lettres **46**, 639 (1985).

[13] M. Rubinstein, Phys. Rev. Lett. **57**, 3023 (1986).

[14] M. E. Cates and J. M. Deutsch, J. Phys. Paris **47**, 2121 (1986).

[15] T. Sakaue, Phys. Rev. Lett. **106**, 167802 (2011).

[16] A. Y. Grosberg, Soft Matter **10**, 560 (2014).

[17] S. Obukhov, A. Johner, J. Baschnagel, H. Meyer, and J. P. Wittmer, EPL **105**, 48005 (2014).

[18] T. A. Kavassalis and J. Noolandi, Macromolecules **22**, 2709 (1989).

[19] A. Rosa and R. Everaers, Phys. Rev. Lett. **112**, 118302 (2014).

[20] J. D. Halverson, W. B. Lee, G. S. Grest, A. Y. Grosberg, and K. Kremer, J. Chem. Phys. **134**, 204904 (2011).

[21] J. D. Halverson, G. S. Grest, A. Y. Grosberg, and K. Kremer, Phys. Rev. Lett. **108**, 038301 (2012).

[22] S. P. Obukhov, M. Rubinstein, and T. Duke, Phys. Rev. Lett. **73**, 1263 (1994).

[23] P. Malo de Molina, A. Alegría, J. Allgaier, M. Kruteva, I. Hoffmann, S. Prévost, M. Monkenbusch, D. Richter, A. Arbe, and J. Colmenero, Phys. Rev. Lett. **123**, 187802 (2019).

[24] B. J. Gold, W. Pyckhout-Hintzen, A. Wischnewski, A. Radulescu, M. Monkenbusch, J. Allgaier, I. Hoffmann, D. Parisi, D. Vlassopoulos, and D. Richter, Phys. Rev. Lett. **122**, 088001 (2019).

[25] J. D. Halverson, W. B. Lee, G. S. Grest, A. Y. Grosberg, and K. Kremer, J. Chem. Phys. **134**, 204905 (2011).

[26] D. G. Tsalikis, T. Koukoulas, V. G. Mavrantzas, R. Pasquino, D. Vlassopoulos, W. Pyckhout-Hintzen, A. Wischnewski, M. Monkenbusch, and D. Richter, Macromolecules **50**, 2565 (2017).

[27] C. P. J. Wong and P. Choi, Soft Matter **16**, 2350 (2020).

[28] C. H. Hövelmann, S. Gooßen, and J. Allgaier, Macromolecules **50**, 4169 (2017).

[29] M. Kruteva, J. Allgaier, I. Grillo, I. Hoffmann, L. Porcar, D. Richter, and R. Schweins, Inst. Laue-Langevin DOI 10.5291/ILL-DATA.9-11-1895 (n.d.).

[30] A. Bensafi, U. Maschke, and M. Benmouna, Polym. Int. **49**, 175 (2000).

[31] G. D. Smith, D. Y. Yoon, R. L. Jaffe, R. H. Colby, R. Krishnamoorti, and L. J. Fetters, Macromolecules **29**, 3462 (1996).

[32] L. J. Fetters, D. J. Lohse, D. Richter, T. A. Witten, and A. Zirkel, Macromolecules **27**,

4639 (1994).

[33] D. G. Tsalikis, P. V. Alatas, L. D. Peristeras, and V. G. Mavrantzas, ACS Macro Lett. **7**, 916 (2018).

[34] E. O. Stejskal and J. E. Tanner, J. Chem. Phys. **42**, 288 (1965).

[35] G. Fleischer and F. Fujara, in *Solid-State NMR I Methods* (Springer Berlin Heidelberg, Berlin, Heidelberg, 1994), pp. 159–207.

[36] B. Mei, Z. E. Dell, and K. S. Schweizer, Macromolecules **53**, 10431 (2020).

[37] M. Guenza, Phys. Rev. Lett. **88**, 4 (2002).

[38] M. Zamponi, A. Weschnewski, M. Monkenbusch, L. Willner, D. Richter, P. Falus, B. Farago, and M. G. Guenza, J. Phys. Chem. B **112**, 16220 (2008).

[39] Z. E. Dell and K. S. Schweizer, Soft Matter **14**, 9132 (2018).

[40] A. Wischnewski, M. Monkenbusch, L. Willner, D. Richter, and G. Kali, Phys. Rev. Lett. **90**, 4 (2003).